STATIC TESTS ON HYBRID PLATE GIRDERS

by

H. S. Lew,

A. A. Toprac

Research Report Number 97-1F

Hybrid Plate Girders Subjected
to Bending and Shear

Research Project Number 3-5-66-97

conducted for

The Texas Highway Department

in cooperation with the
U. S. Department of Transportation
Federal Highway Administration
Bureau of Public Roads

by the

CENTER FOR HIGHWAY RESEARCH

THE UNIVERSITY OF TEXAS

AUSTIN, TEXAS

July 1967

ACKNOWLEDGMENTS

The tests described herein were conducted as a part of the overall research program at The University of Texas, Center for Highway Research under the administrative direction of Dean John J. McKetta. The work was sponsored jointly by the Texas Highway Department and the Bureau of Public Roads under an agreement between The University of Texas and the Texas Highway Department. Liaison with the Texas Highway Department was maintained through the contact representative, R. Vanderstraten.

The research work has been conducted at the Structures Fatigue Research Laboratory, The University of Texas, under the direction of Professor A. A. Toprac.

The project staff included Messers. B. R. Karrh, L. D. Long, D. G. Eyre, and H. Toyoda. Their assistance in conducting the tests and in compiling earlier reports is gratefully appreciated.

PREFACE

This report describes the static tests of six hybrid plate girders comprised of A514 steel flanges and A36 steel web. Five specimens were tested under pure bending and one under high shear. The objectives of the bending tests were to provide information on the buckling behavior of the compression flange as it is affected by the yielding in the web and to determine experimentally the ultimate loads and to compare them with reference values computed on the basis of elastic and plastic beam theory. The purpose of the shear tests was to investigate how well the current ultimate shear-strength theory predicts the actual strength determined by tests.

Web slenderness ratios and flange width-to-thickness ratios were variables considered in the bending tests. For the shear tests, only the transverse stiffener spacing was varied. The behavior of each girder is described in the test and the results are presented. Conclusions on the results of the experimental studies are reported.

The opinions, findings, and conclusions expressed in this publication are those of the authors and not necessarily those of the Bureau of Public Roads.

TABLE OF CONTENTS

PART 1: TEST PROGRAM

1.1 Introduction

The purpose of Part 1 is to describe the test specimens and to present the chemical and physical properties of the material used, the girder dimensions, and computed reference loads based on actual measurements.

A total of six specimens made of constructional alloy steel flanges and low carbon steel webs were tested to ultimate load; five were subjected to pure bending and one to high constant shear. Figure 1.1 shows schematically these two loading conditions. Five bending tests were made on panel specimens, with one test conducted on each specimen. While the panel aspect ratio (ratio of panel width to web depth) was kept constant for all test specimens, both the web slenderness ratios (ratio of web depth to web thickness) and to flange width-to-thickness ratios were varied. Each bending specimen was connected to two loading fixtures whose structural rigidity was considerably greater than that of the test specimens, thus permitting their reuse for all bending tests.

Three static shear tests were conducted on a full-length specimen. In the shear tests, while the web slenderness ratio and flange dimensions were kept constant, the panel aspect ratio was varied. The specimen had three different panel widths. By repairing the failed panel (or panels) which had a larger aspect ratio than the remaining panels, it was possible to conduct three tests. Figure 1.2 shows test sequences and positions of the repaired stiffeners in the panel that failed.

1.2 Girder Dimensions

Nominal dimensions of both bending and shear test specimens are shown in Figs. 1.3 and 1.4, respectively. For cross-sectional properties, actual dimensions were used. Thicknesses of component plates of the specimens were obtained from coupons, which were cut from the same plates that were used for fabrication of the specimens, and the flange width was measured at along the flanges. Nominal dimensions were used for web depth and spacing of the transverse stiffeners. The values of the geometric parameters used as variables are listed in Table 1.1 and measured cross-sectional dimensions are listed in Table 1.2.

1.3 Material Properties

Standard tensile tests were conducted to obtain the mechanical properties of the component plates of the test specimens. The properties are listed for each component plate of the girders in Table 1.3 with the chemical properties as they appeared in the mill test reports.

Yield stresses in this table were obtained under zero strain rate, and these values were used in calculating reference values. To obtain an average value of the yield stress, two tensile tests were made from each coupon plate. For the web one specimen was cut from the coupon plate in the direction parallel to rolling and the other perpendicular to rolling, whereas for the flange two specimens had to be taken from the coupon plates parallel to the direction of rolling. Percent elongation over an 8-in. gage length was measured to indicate ductility.

1.4 Reference Loads

For the bending specimens four reference loads were evaluated. They were P_{crb}, P_{yw}, P_{yf}, and P_p. The load, P_{crb}, which corresponds

to the critical elastic buckling stress, σ_{cr}, at which a plane web panel buckles into wavy form, is expressed as

$$P_{crb} = \frac{\sigma_{cr} \cdot S}{120 \text{ (in.)}} \tag{1}$$

where

$$\sigma_{cr} = k_b \frac{\pi^2 E}{12 (1-\nu^2)} \left(\frac{w}{h}\right)^2 \tag{2}$$

120 in. = moment arm,
S = section modulus,
ν = Poisson's ratio.

In the above expression w and h are web thickness and web depth, respectively, and k_b is a buckling coefficient for pure bending equal to 23.9 for simply supported edges.[1]

P_{yw} and P_{yf} are defined as the loads which cause initiation of yielding at the extremes of the web and flange, respectively. Both reference loads are given by

$$P_{yw} = \frac{1}{120} \sigma_{yw} \left(A_f + \frac{A_w}{6}\right) h \tag{3}$$

$$P_{yf} = \sigma_{yf} A_f h + \sigma_{yw} A_w \left[1 - \frac{1}{3}\left(\frac{\sigma_{yw}}{\sigma_{yf}}\right)^2\right] \frac{h}{4} \tag{4}$$

where

σ_{yw} = yield point of web,
σ_{yf} = yield point of flange,
A_f = area of flange, and
A_w = area of web.

P_p is the load which causes the plastic moment M_p of simple plastic theory. Thus, P_p is obtained from

$$P_p = \frac{M_p}{120(\text{in.})} \tag{5}$$

in which

$$M_p = \sigma_{yf} A_f h + \sigma_{yw} A_w \frac{h}{4}$$

For the shear specimens three reference loads were given. They were P_{crs}, P_u, and P_{ys}. The load, P_{crs}, which corresponds to the critical elastic buckling stress τ_{cr} at which a plane web panel buckles due to shear alone is given by

$$P_{crs} = \tau_{cr} A_w \tag{6}$$

where

$$\tau_{cr} = k_s \frac{\pi^2 E}{12(1-\nu^2)} \left(\frac{w}{h}\right)^2 \tag{7a}$$

and

$$k_s = 5.34 + \frac{4.00}{\alpha^2} \qquad \text{for } \alpha \geq 1 \tag{7b}$$

$$k_s = 4.00 + \frac{5.34}{\alpha^2} \qquad \text{for } \alpha \leq 1 \tag{7c}$$

Web buckling coefficients k_s are obtained under the assumption that the web panels are simply supported on all edges.[1] The panel aspect ratio α is the ratio of panel width to depth, i.e., a/h.

The theoretical ultimate load P_u is computed according to Ref. 2, while the plastic shear load P_{ys}, similar to P_p of bending, is equal to

$$P_{ys} = \tau_y \cdot A_w \tag{8}$$

where τ_y is equal to $\sigma_y/\sqrt{3}$ according to von Mises' yield condition. The reference loads for each test specimen based on the above equations and theory are listed in Tables 1.4 and 1.5.

PART 2: BENDING TESTS

2.1 Introduction

Both experimental investigations[3] and theoretical studies[4] have shown that the ultimate strength of homogeneous girders* subjected to pure bending is limited by the failure of the compression flange. The buckling of the compression flange can be categorized into three basic modes: (1) vertical buckling, (2) torsional buckling, and (3) lateral buckling.

In homogeneous girders the applied longitudinal bending stress is a maximum at the extreme fibers of the flanges, and yielding initiates from those fibers. Thus, the ultimate strength as determined by the instability of the compression flange is based on the assumption that the entire cross-section remains elastic prior to failure. In contrast to this, in hybrid girders, yielding begins in the web at the flange-web juncture under a lower load than that required to cause yielding in the flanges. Thus, the behavior of hybrid girders may differ from that of homogeneous girders under pure bending.

The objectives of the tests carried out were, therefore;

(1) to study the effect of yielding in the web on the behavior of the compression flange, and

(2) to determine experimental ultimate loads and to compare these with the reference values mentioned in Sect. 1.4.

---

*Homogeneous girder cross section comprised of steels having the same physical properties.

2.2 Test Specimens

Since lateral buckling is resisted primarily by the compression-flange column, the behavior of the compression flange in this mode of failure is the same for both homogeneous and hybrid girders. Thus, a study of this mode of failure was eliminated from the present tests. To investigate the vertical and local-torsional buckling of the compression flange, both web and flange thicknesses were varied. The web thickness was varied from 11 gage (0.1196 in.) to 1/4 in. and the flange thickness was varied from 1/4 to 3/8 in.

All five test specimens had an overall length of 8 ft. with the test panel length of 4 ft. 6 in. in the middle. The test panel was isolated by two pairs of transverse stiffeners. The stiffeners were designed conservatively and were cut 3/4 in. short of the tension flange. Web depth was kept constant at 3 ft. thus providing nominal web slenderness ratios, ranging from 144 to 301.

2.3 Test Setup

By applying the loads directly to the loading fixtures (see Part 1 and Figure 1.1), only bending moment was transferred to the test specimen. In the joints between the loading fixtures and the specimen, 1-1/8-in.-diameter and 7/8-in.-diameter A-490 (high strength) bolts were used for flange and for web connections, respectively.

The loading system consisted of two 200-kip capacity Simplex hydraulic jacks, one applied on each loading fixture. By supplying oil to each jack through a manifold, it was possible to maintain an equal oil pressure in the loading system. The magnitude of load at each jack was monitored by load cells connected to a strain indicator.

In order to permit the loading jacks to rotate with the girder as it deflected under the load, the system shown in Fig. 2.1 was used.

To prevent lateral buckling of the compression flange, intermittent lateral supports were provided by 2-in.-diameter steel pipes with a ball and socket joint at each end. This system was designed so that the girder could move only vertically (see Fig. 2.2).

2.4 Instrumentation

During the tests, both deflection and strain readings were procured. Vertical deflections were measured with two independent systems. The first system consisted of an engineer's level and scales mounted at various points on the girder. The second system consisted of dial gages placed at several locations including the positions where the scales were located.

To measure the inital web configurations and subsequent deflected shapes under load, a special dial rig with movable head was used (Fig. 2.3). By moving both the head vertically at 3-in. intervals and the rig along the girder axis 3-in. intervals, it was possible to establish the deflections of the entire web panel at 3-in. by 3-in. grid points.

Electrical resistance strain gages, placed in pairs (one on each side of the web plate), were used to measure the direct membrane (axial) strains and bending strains due to lateral deformation of the web. All strain gages were located in the center portion of the test panel, as previous experience has indicated that the crest of a buckle wave generally occurs at that region.

In order to detect any twist of the compression flange, pairs of dial gages were placed within the test section at 6-in. intervals (Fig. 2.4) and 1/2 in. away from the edges of the compression flange.

To obtain a visual qualitative indication of the location and extent of strains, all test girders were whitewashed prior to testing.

2.5 General Girder Behavior

The general behavior of a girder can be traced by a load-deflection curve. Load versus deflection at the center of the test panel, which is also the center of the test girder, is plotted for each girder, as shown in Figs. 2.5 through 2.9. The plotted deflection was obtained from measurements taken with a dial gage placed at the center of the test panel and was corrected for end-support settlements. In order to eliminate the possibility of slip at the bolted joints under large loads and to ensure complete bearing between bolts and plates, the test girder was first loaded to about 10 kips prior to tightening the bolts. After tightening the bolts, the test specimen was unloaded so that initial readings could be taken. Subsequent measurements were taken at predetermined load increments, and for ease of reference each load level was numbered in ascending order with the initial zero load labled as load No. 1.

To make the load versus deflection curves more meaningful, the reference loads given in Table 1.3 are indicated on each figure. A thin solid line shown in each figure is the elastic deflection curve and applicable only up to P_{yw}. When the load versus deflection curves (plotted during tests) deviated from a straight line, all measurements were made after the load became stabilized.

2.6 Cross-Section Strain Distribution

In order to examine strain distribution throughout the depth of each girder, longitudinal strain measurements were taken at various points.

The strains were measured at each load increment at the center line of the test panel by means of electrical resistance strain gages. As mentioned previously, two strain gages were placed at these points on either side of the web to obtain membrane strains.

The longitudinal strain distributions at four selected loads are plotted in Figs. 2.10 through 2.14. The positions of strain gages are indicated by thin solid lines on the web across the girder profile.

The longitudinal strains and those predicted by beam theory (Mc/I), are shown in Figs. 2.15 through 2.19. In these figures the strain is plotted as the abscissa and the load P as the ordinate.

2.7 Flange Strain Distribution and Rotation

For all five test girders both the strain distribution in the compression flange and the flange rotations along the girder axis were measured. The flange strains were measured at the center section of the test panel and are shown in Fig. 2.20. The rotations of the compression flange measured at 6-in. intervals in the middle portion of the test panel are shown in Figs. 2.21 through 2.25. In these figures the rotation is given in radians, considered positive when rotated counterclockwise as shown in the figures. The purpose of measuring the flange rotations was to investigate the behavior of the compression flange and to detect the onset of torsional buckling of the compression flange.

2.8 Web Deflections

The purpose of lateral web deflection measurements was to determine the deflection of the web out of its plane. For all five girders the initial out-of-straightness of the test panels was measured. In addition to

the initial readings, at least one more set of readings was taken at a higher load to observe changes in the web deformations under an increasing load. The lateral deformations are presented in Figs. 2.26 through 2.30, superimposed on cross-sectional profiles.

2.9 Ultimate Loads and Modes of Failure

Girder HB-1

Yielding in the compression side of the web was first observed at Load No. 7 (60 kips). The ultimate load was 129 kips. Failure was brought about by vertical buckling of the compression flange, which occurred instantaneously without any visible warning. Figure 2.1 shows an overall appearance of the failed panel.

Girder HB-2

Because HB-1 exhibited an early deviation from the elastic deflection curve, this girder was loaded twice to see whether risidual stresses produced during the fabrication were the reason for such deviation. Yielding of the web near the compression flange was first observed at load No. 3 during the first cycle. The load was increased to Load No. 4 and then the girder was unloaded to zero kips. It is seen in Fig. 2.6 that in the second cycle of loading, the deflection curve remained linear up to Load No. 10 which was the same load level as Load No. 4 of the first cycle. This indicates that the nonlinearity of the deflection curve of HB-1 can be attributed to the residual stresses.

The ultimate load of this girder, 140 kips, was limited by vertical buckling of the compression flange. Figure 2.32 shows an overall deformation of the test panel and the extent of yielding in the tension zone of the web.

Girder HB-3

Yielding in the compression flange was first observed at Load No. 15 and occurred only on one side of the compression flange. A gradual twisting of the compression flange near the center of the panel was noted between Loads No. 15 and 16. The ultimate load was 129 kips and, unlike the first two girders, the failure was brought about by torsional buckling of the compression flange.

Figure 2.33 shows the appearance of the test panel after failure.

Girder HB-4

Twisting of the compression flange was noted at Load No. 3, and between Loads No. 4 and 5 yield lines appeared in the web near the compression flange. A considerable rotation of the compression flange took place before Load No. 8 (55 kips) and no further increase in the jack load was possible beyond this point. An inspection of the test panel revealed that although there was a pronounced local buckle wave in the compression flange, no yield lines were noted in the flange. Further application of load caused the load to drop to Load No. 9 (refer to Fig. 2.8). Since it appeared that the girder had reached the ultimate load, the girder was unloaded to zero kips.

Figure 2.34 shows an overall view of the test panel after failure and a detailed view of the flange rotation.

Girder HB-5

First yielding of the web in the compression side was observed between Loads No. 2 and 3. As a result of early yielding in the web, the deflection curve also deviated from a straight line. Rotation of the

compression flange was noted at Load No. 4 and it increased gradually with increasing load. The ultimate load of 80 kips was attained at Load No. 10 with the compression flange severely twisted. The test panel after failure is shown in Fig. 2.35.

2.10 Discussion of Test Results

Failure Modes

The measured ultimate loads P_{ex} are listed in Table 2.1 together with the values of the web slenderness ratio β and the flange width-to-thickness ratio b/t based on the actual measured dimensions. In order to compare the experimental values with theoretical ones, ratios of P_{ex} to the reference loads given in Table 1.4 are computed and are listed in the same table. The last column of this table gives the mode of failure of each girder.

One of the objectives of the tests was to ascertain at what value of the β-ratio vertical buckling of the compression flange takes place prior to other modes of failure. It is seen from Table 1.4 that vertical buckling of the compression flange did occur in two specimens (HB-1 and HB-2) whose β ratios were 305 and 277, respectively, and had a b/t ratio of 8.0. For HB-3, which had the same b/t ratio (8.0) but had a β ratio of 188, the failure mode was torsional buckling of the compression flange instead of vertical buckling. Thus, the tests indicate that a hybrid girder whose β ratio is higher than 188 may fail due to vertical buckling of the compression flange.

Three test girders (HB-3, HB-4, and HB-5) failed due to torsional buckling of the compression flange. Strain readings (Figs. 2.17, 2.18 and 2.19) indicate that only in HB-3 had the flange strain exceeded the yield strain of the flange while the flange strains in HB-4 and HB-5 remained

below the yield strain. It is seen in Table 1.4 that for HB-3, which had a b/t ratio of 8.0, the ultimate load was 99 percent of P_{yf}, whereas for HB-4 and HB-5, which had b/t ratios of 15.54 and 10.85, the ultimate loads were only 58 and 67 percent of P_{yf}, respectively. Furthermore, a comparison of b/t ratios indicate that in order not to have the flange buckle torsonally, the flange width-to-thickness ratio should be less than 8.0. This is contrary to the test results on welded cruciform sections of A514 steel,[5] which had a similar buckling mode as the compression flange of hybrid girder. In the test of Ref. 5 it was found that a b/t ratio of 10.0 would be sufficient to insure that the compression flange would reach the yield stress without torsional buckling. However, other test results on hybrid girders[6] agree well with a limiting b/t ratio of 8.0 rather than the 10.0 obtained from the cruciform tests.

Strain Distribution

As shown in Figs. 2.10 to 2.14, in all cases the strains in the compression region of the web were less than those predicted by simple beam theory. Previous research on homogeneous plate girders[3] has shown that this loss of strains was attributed to lateral deflections of the web, which caused the web to take less than its proportional share of the beam theory strain. The amount of the loss is difficult to estimate because it also depends on the magnitude of lateral web deflections, but the strain distributions for all girders except HB-4 indicate that the longitudinal bending strain in the web at 1/4 of the depth below the compression flange remained relatively constant beyond a certain load. This trend can also be seen in Figs. 2.15 through 2.19 in which the strains in the compression zone of the web did not increase after 30 percent of the respective ultimate load.

A previous study on homogeneous girders[4] demonstrated that the loss of strains in the web allowed stress redistribution from the web to the compression flange to maintain an equilibrium in the cross section. Such redistribution of stresses results in increased compression flange stresses above the one computed by beam theory. However, strains plotted for the compression and tension flange shown in Figs. 2.10 to 2.14 indicate that the results were not consistantly in agreement with the conclusion drawn from the homogeneous girder tests. One of the reasons for the lack of agreement is due to the fact that the ratio of moments carried by web to flange in a hybrid girder is much less than that of a homogeneous girder having the same cross-sectional dimension.

Lateral Web Deflections

Lateral web deflections plotted on a profile of the girder cross section are shown in Figs. 2.26 through 2.30. These figures show that the configuration and magnitude of the initial web deflections varied from girder to girder. The maximum measured initial out-of-straightness for HB-1 and HB-2 was 4.64 and 4.45 times the web thickness, respectively, while both HB-3 and HB-4 had initial crookedness of 1.83 times their web thicknesses. HB-5 was the only specimen which had the initial out-of-straightness equal to the thickness of its web.

In all cases, however, subsequent deflections at higher loads did not increase much from the original deformed shape. In fact, it has been shown in other investigations[7] that as the deflections increase with loading, tensile membrane stresses develop in the web orthogonal to the girder axis. The stresses, in turn, then limit the growth of the deflections, and consequently the deflections in the elastic range never exceed a low multiple of

the plate thickness. This evidence has also been shown by the longitudinal strain measurements (Figs. 2.15 to 2.19) where the strains in the compression part of the web remained constant after increasing to a certain value. Thus, this evidence indicates that the magnitude of stress transfer from the web to the compression flange is, to a certain extent, limited.

Compression Flange Rotation

The onset of local buckling in the compression flange of the test girders was indicated by rotational twisting of the flange (Figs. 2.21 through 2.25). These figures reveal that in those specimens which failed by local buckling the final flange rotations were much greater than in those which failed by vertical buckling in which the compression flange crashed into the web.

The specimens which failed by vertical buckling indicated that rotations increased under the initial loading stage (up to about 30 percent of the failure load) and then remained relatively constant until the final loading stage was reached. During the final loading stages the rotations actually decreased (Figs. 2.21 and 2.22). The specimens which failed by local buckling presented a type of flange behavior similar to what would be expected in beam tests. In general, the rotations were almost linear with respect to the applied load until near the ultimate load. However, a comparison of the flange rotations of HB-3 (Fig. 2.25) and HB-5 (Fig. 2.25) indicates that the compression flange of HB-3, which had a b/t ratio of 8.0, remained undistorted until near the ultimate load, whereas the flange of HB-5, which had a b/t ratio of 11.0, began to rotate considerably from the initial stage of the test.

In all cases, once the local buckle had formed in the compression flange of a girder, the ultimate load had been reached. Upon further straining, the flange underwent further distortion.

2.11 Conclusions

Based on the five bending tests reported herein, the following conclusions can be drawn:

(1) In all girders, the ultimate load exceeded the web yield load by a substantial margin, depending primarily on the b/t ratio of the compression flange (see Table 2.1).

(2) As a result of lateral web deflections, the strains in the compression part of the web did not increase as predicted by beam theory but remained constant after increasing to a certain value.

(3) The test results indicate that a limiting value of the β ratio against vertical buckling can be estimated as $188 \leq \beta < 277$.

(4) The test results of HB-3 and HB-5 have shown that a limiting value of the b/t ratio is closer to 8.0 rather than 10.0, which is based on the test results of cruciforms.

PART 3: SHEAR TESTS

3.1 Introduction

For transversely stiffened homogeneous plate girders subjected to high shear it has been shown that a significant post buckling strength is attained through the development of tension-field action.[2] Since the tension-field stresses are assumed to be anchored to transverse stiffeners, and since the web is assumed to carry all the beam-type shear force, the role of the flanges in resisting the shear force is neglected in the derivation of the shear-strength formula. Under high shear load, therefore, the flanges serve only to resist the concurrent moment and as framing elements for the web panel.

In hybrid girders the flange area tends to be smaller than the flange area of homogeneous girders because the flange yield point is higher than that of the web. Consequently, the rigidity of the flanges is reduced at the same time. Such a reduction may cause premature failure of the flanges, as framing members of the web panel, due to an excessive shear deformation. Accordingly, the objectives of this part of the investigation were

(1) to investigate how closely the current ultimate shear strength theory predicts the actual strength, and

(2) to explore the influence of relatively smaller flanges on the strength of the web panel.

3.2 Test Specimen

As mentioned in Part 1, the test girder had three different widths of transverse spacing: 72, 36, and 18-in. Thus, for a constant web depth

of 36 in., these stiffener spacings yielded panel aspect ratios of 2.0, 1.0, and 0.5. With one test panel of $\alpha = 2.0$, two test panels of $\alpha = 1.0$, eight test panels of $\alpha = 0.5$, and a 6-in.-wide end post at each end of the girder, the test specimen had an overall length of 25 ft. The arrangement of the test panels is shown in Fig. 1.4.

Transverse stiffeners were designed according to the current AISC specifications[8] and were cut 3/4 in. short of the tension flange. In order to exclude the possibility of a premature failure of end panels, the end posts were designed conservatively, exceeding the design procedure suggested in Ref. 8.

3.3 Test Setup

Test setup is shown in Fig. 3.1. The loads were applied by means of two 200-kip capacity hydraulic jacks at each end. The lower support with a rocker plate provided hinged-support condition, while the upper support with a cylinder between the girder and a stub column provided roller-support condition. The magnitude of load at each end was monitored by load cells which together with the jacks were held in position by a steel cannister system as shown in Fig. 3.1.

The compression flange was braced by the same system as used for the bending tests (Sec. 2.3). In addition to these, lateral supports were also placed at the load points and at the upper support. Figure 3.2 shows loading arrangements, lateral bracings, and the upper support.

3.4 Instrumentation

In general, there were three categories of data taken during the testing, i.e., vertical girder deflections, lateral web deformations, and strains in the web and the flanges.

Vertical girder deflections were taken so that the general behavior of the specimen could be followed as testing proceeded. Deflections were read by two independent methods to serve as a cross check. The first method consisted of a set of 0.001 in. dial gages, and the second method consisted of an engineer's level and a set of scales graduated to 1/100 in. placed along the girder. Lateral web deflections were read by the same dial rig as used in the bending tests and measurements were taken at 3-in. interval grid points as described in Sec. 2.4.

Web and flange strains were measured with electrical strain gages. Right-angle-rosette strain gages were used on the web surface, one on each surface of the web so that membrane and bending strains could be separated. The purpose of using these rosettes was to determine the direction and magnitude of the principle strains. Uniaxial gages were used on the flange surfaces to serve as a check on the strain distribution due to flexure. For visual observation of yielding, the girder was coated with whitewash prior to testing.

3.5 Testing Procedure

Testing was started by taking readings on all instruments at zero load. The load was then increased in predetermined increments with data being recorded after each load increment. This procedure was continued until inelastic behavior of the girder was observed as indicated by a substantial increase in deflection with a small increase in load. Thereafter, several minutes were allowed to elapse before the instrument readings were taken. This inelastic behavior could usually be observed also by flaking of the whitewash in the area of yielding. Upon observing the inelastic behavior, the girder was unloaded to zero kips. This completed

the first cycle of loading. The purpose of this first cycle was to eliminate most of the residual stress effects from the strain gage readings. In the second cycle the load was increased in increments to failure of the panel being tested. The first test (T1) was terminated with the removal of the load.

The first test was completed with the failure of the 72-in. panel and the panel was then reinforced by trimming and welding 3/16-in.-thick vertical stiffeners at 12-in. intervals onto each side of the deformed web as shown in Fig. 1.2b.

The same testing procedure was then repeated so as to produce a failure in one of the two 36-in. panels (T2), both of which were then reinforced as described previously for the 72-in. panel as shown in Fig. 1.2c. The 18-in. panels were then tested to failure (T3) with only vertical dial gage and engineer's level readings being taken.

3.6 General Girder Behavior

The general behavior of a girder can be depicted by a load-deflection diagram. For each test the applied load versus girder end deflection is plotted and shown in Fig. 3.3. Since both ends deflected about the same amount, only the deflection where the load was applied downward is presented. Three reference loads shown in the figure are those given in Table 1.4. Two cycles of loading were conducted for each test (T2 and T3) but, because the curves for the first and the second load cycles are approximately equal, only the curve for the second cycle is shown.

Test T1. During the first test, attention was focused primarily on the longest test panel of $\alpha = 2.0$, where the failure was expected to occur. Although no visible signs of yielding were noted, the deflection curve

departed from a straight line after Load No. 3 (Fig. 3.3). The first sign of yielding along the tension diagonal was observed between Loads No. 7 and 8. When Load No. 9 was reached, yielding was evident along the diagonal, as shown in Fig. 3.4. At this point the girder was unloaded to Load No. 15 (zero load) and was immediately followed by the second cycle of loading. It is seen in the figure that in the second cycle of loading the deflection curve remained linear up to Load No. 18. Upon further loading, the deflection curve deviated immediately from the straight line and traced the path of the first loading cycle up to Load No. 19. Beyond this point it was not possible to increase the load any further, and the load dropped to Load No. 20 with a considerable deflection. An excessive deformation of the test panel was also noted at this time with both flanges drawn together as much as 1/2 in. Judging from the deflection curve, it was apparent that the ultimate load had been reached during the first cycle of loading. The girder was then unloaded to reinforce the failed panel.

Test T2. Up to Load No. 32 (90 kips) the deflection curves of the first and second cycles of loading followed the same path. There was an indication of yielding in both test panels between Loads No. 38 and 39. As shown in Fig. 3.5, this yielding became more pronounced by the time the ultimate load of 125 kips (Load No. 41) was reached. It should be noted in this figure that unlike the previous test panel (α = 2.0) wherein the tension diagonal formed from one corner of the panel to the opposite corner, in these panels (α = 1.0) the yield band started from one corner of the compression region and terminated about 1/2 of the web depth above the tension flange.

After reaching the ultimate load, the girder was unloaded to zero kips (Load No. 48) to reinforce the two failed panels.

Test T3. The load versus deflection curve indicates that the third test behaved very much the same as the second test. However, the final failure was brought about by extensive diagonal yieldings in one end of the girder while the other end showed almost no sign of any diagonal yielding. Figure 3.6 shows the mode of failure and the yield bands in the last two panels near the load point.

3.7 Web Deflections

Results of lateral web deflection measurements are presented as deflection contours of test panels and as profiles of girder cross sections spaced at 3-in. intervals. In both schemes the deflections were plotted relative to the panel boundaries, which were assumed to have no deflection.

For T1, Fig. 3.7 shows both contours and profile plots at Loads No. 1 and 9 (0 kip and 98 kips), and for T2, Fig. 3.8 shows the same at Loads No. 28, 37, and 40 (0 kip, 80 kips, and 120 kips). Because both test panels of T2 exhibited the same deformed shape and deflections in the same order of magnitude, only the deflection plots of the panel next to the 72-in. panel are presented. No deflection measurements were taken during T3.

3.8 Web Strains

Figures 3.9 and 3.10 show the change in magnitude of the principal stresses and their directions with increase in load for T1. Figures 3.11 to 3.17 show the same for T2. In these figures the maximum principal stresses are shown as hollow circles and the minimum principal stresses as solid circles. Dashed lines indicated the theoretical values based on beam theory. If principal strains exceeded the yield strain of the web, the corresponding stresses are plotted as the yield stress.

3.9 Discussion of Test Results

The measured ultimate loads P_{ex} are listed in Table 3.1, together with β and α ratios. For comparison, ratios of P_{ex} to the reference loads given in Table 1.5 are computed and are listed in the last three columns of Table 3.1. It is obvious from the values of P_{ex}/P_{crs} and P_{ex}/P_y that both elastic shear buckling load and beam-theory yield load do not provide an accurate prediction of the shear strength. In the last column of this table are listed the ratios of the experimental ultimate loads to the theoretical ultimate loads, P_{ex}/P_u calculated according to Ref. 2. It is seen that the theory overestimates the failure load of the panel with $\alpha = 2.0$ by 7 percent, while it underestimates the failure loads of $\alpha = 1.0$ and $\alpha = 0.5$ panels by 6 and 4 percent, respectively. Similar discrepancies were also observed in homogeneous girder tests (see Table 1 of Ref. 2), in which the ratio P_{ex}/P_u ranges from 0.88 to 1.12.

Lateral Web Deflections

Both contours and profile plots revealed that deflection valleys, or buckles, were formed as a result of the compressive stresses in the web. Thus, the axes of the buckles are usually perpendicular to the compressive stresses, and the magnitude of the tensile stress is a maximum at the crests of the buckles.

In $\alpha = 2.0$ panel, Fig. 3.7 shows that one large diagonal buckle formed along the tension diagonal of the panel, extending from one corner to the opposite corner. A photograph taken after failure (Fig. 3.4) shows a dark yield band along the tension diagonal revealing extensive yielding in that direction. In $\alpha = 1.0$ panels, however, although the buckles formed in the panels, the angle of inclination of the buckles was much less than the

angle of the panel diagonal. Such orientation of the buckles does not conform to the ones observed in homogeneous girder tests,[3] i.e., in nearly square panels the buckles usually extended from corner to corner. In any case, the yield bands formed along the crests of the buckles indicate that tension-field action did develop in the test panels.

Web Stresses

Although reasonably good agreement between the experimental ultimate loads and Basler's solution[2] indicates that the ultimate strength theory based on tension-field action could be used to predict the ultimate load of hybrid girders, it is of interest to examine the mechanics of the tension-field action developed in the test panels.

Tension-field action basically says that compressive diagonal stresses increase until the critical web buckling stress is reached, at which time the web buckles. Thereafter, while the tension diagonal stresses increase, the compressive diagonal stresses remain essentially constant. Plots of the load versus the principal stresses for each location of rosette gages (Figs. 3.9 to 3.17) reveal that only the principal stresses at the center of the $\alpha = 2.0$ panel (Fig. 3.10) showed this behavior. It is seen that, above the critical buckling load P_{crs}, while the compressive principal stress remained below the theoretical stress, the tensile principal stress increased to about twice the theoretical stress near the ultimate load. The orientation of the tensile principal stress also changed from the theoretical value of 45 degrees toward the panel diagonal angle of 22.5 degrees. These measurements of the principal stresses and angular rotations indicate that the diagonal tension-field was highly developed in the $\alpha = 2.0$ panel.

In the α = 1.0 panel, whereas the compressive principal stress at the center of the panel remained relatively constant above the critical buckling load P_{crs}, the tensile principal stress followed the theoretical value very closely. In fact, tensile principal stresses at other locations did not deviate much from the theoretical values. Except in one other location (Fig. 3.21) where the compressive principal stress remained constant and decreased near the ultimate load, all compressive principal stresses were larger than the theoretical values. Since most of these gages were located near the boundary members of the web panel, the strain readings were undoubtedly affected by forces in these members. However, inclinations of the tensile principal stress at two diagonally opposite corners (refer to Figs. 3.11 and 3.17) near the ultimate load indicate that the tension-field stress anchored at only one of these corners, for the angle between the tensile principal stress and the horizonal axis at the upper corner was 30.5 degrees, while the angle at the lower corner was 47 degrees. Fig. 3.5 shows that the tension-field was anchored at the upper corner where the yield band along the valley of the buckle extended from the upper corner to the mid-depth of the panel.

3.10 Conclusions

Based on the test results presented the following conclusions may be drawn:

(1) For hybrid girders subjected to high shear, tension-field theory could be used to predict the ultimate load.

(2) Tension diagonal yield bands do form in web panels, but such yield bands may not extend from one corner of a panel to the diagonally opposite corner.

(3) Use of relatively smaller flanges may not be a problem in hybrid girders, as the experimental ultimate load of the α = 2.0 panel, which had the flanges drawn together as much as 1/2 in., exceeded the theoretical value.

REFERENCES

1. Bleich, F.,
   BUCKLING STRENGTH OF METAL STRUCTURES,
   McGraw-Hill, New York (1952).

2. Basler, K.,
   STRENGTH OF PLATE GIRDERS IN SHEAR,
   Proc. ASCE, 87, No. ST7, 1961.

3. Basler, K., Yen., B. T., Mueller, J. A., and Thürlimann, B.,
   WEB BUCKLING TESTS ON WELDED PLATE GIRDERS,
   Bul. No. 64, Welding Research Council, 1960.

4. Basler, K., and Thürlimann, B.,
   STRENGTH OF PLATE GIRDERS IN BENDING,
   Proc. ASCE, 87, No. ST6, 1961.

5. Haaijer, G.,
   DEVELOPMENT OF RESEARCH DATA FOR USE IN STEEL DESIGN,
   U.S. Steel Corporation, Applied Research Lab.
   Tech. Report 57.019-901(2), 1964.

6. Toyoda, H.,
   STATIC BEHAVIOR OF HYBRID PLATE GIRDERS,
   M.S. Thesis submitted to The University of Texas, 1967.

7. Rockey, K. C. and Jenkins, F.,
   THE BEHAVIOR OF WEB PLATES OF PLATE GIRDERS SUBJECTED TO PURE BENDING,
   Struct. Engn., Vol. 36, 1957.

8. AISC
   SPECIFICATION FOR THE DESIGN, FABRICATION AND ERECTION OF STRUCTURAL STEEL FOR BUILDINGS,
   AISC, New York, 1963.

GIRDER	$\alpha = \frac{a}{h}$	$\beta = \frac{h}{w}$	$\frac{b}{t}$	Material Specification (Flange/Web)	LOADING
HB-1	1.5	300	8.0	A514/Sheet Metal	BENDING
HB-2	1.5	269	8.0	A514/Sheet Metal	
HB-3	1.5	192	8.0	A514/A36	
HB-4	1.5	144	16.0	A514/A36	
HB-5	1.5	144	10.7	A514/A36	
HS-1A T 1	2.0	192	8.0	A514/A36	SHEAR
HS-1A T 2	1.0	192	8.0		
HS-1A T 3	0.5	192	8.0		

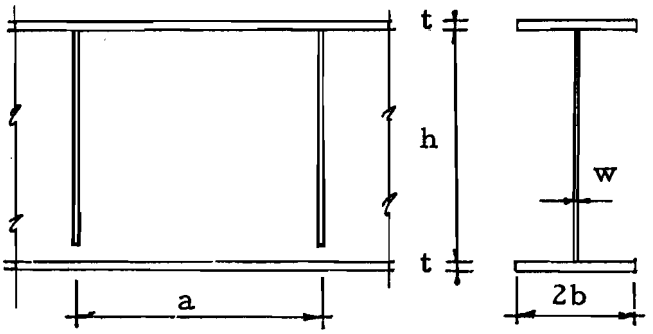

TABLE 1.1 Geometric Parameters and Flange-Web Steels

GIRDER	FLANGE + (in.)	WEB (in.)	I ($in.^4$)
HB-1	0.502 x 7.978	0.118 x 36.00*	3162.91
HB-2	0.502 x 8.008	0.130 x 36.00*	3183.56
HB-3	0.502 x 8.025	0.191 x 36.00*	3426.45
HB-4	0.259 x 8.051	0.247 x 36.00*	2331.06
HB-5	0.370 x 8.029	0.247 x 36.00*	2925.12
HS-1A	0.533 x 7.988	0.187 x 35.87	3545.43

+ Flange width is given as an average of Tension and Compression flange

* Nominal Dimension

TABLE 1.2 ACTUAL DIMENSIONS OF COMPONENT PLATES

GIRDER	Components	Specification	σ_y (KSI)	σ_u (KSI)	% Elong. in 8-in.	CHEMICAL PROPERTIES (in %)					
						C	Mn	P	S	Cu	Si
HB-1	Flange	ASTM A514	107.61	119.51	13.28	0.200	0.590	0.010	0.018		0.280
	Web	Sheet Metal	33.88	46.82	29.71	Not Available					
HB-2	Flange	ASTM A514	107.61	119.51	13.28	0.200	0.590	0.010	0.018		0.280
	Web	Sheet Metal	34.63	46.10	27.56	Not Available					
HB-3	Flange	ASTM A514	107.61	119.51	13.28	0.200	0.590	0.010	0.018		0.280
	Web	ASTM A36	38.31	60.58	30.64	Not Available					
HB-4	Flange	ASTM A514	113.69	117.31	22.90	0.160	0.580	0.012	0.016		0.270
	Web	ASTM A36	35.82	54.63	31.58	Not Available					
HB-5	Flange	ASTM A514	108.27	115.95	12.38	0.190	0.560	0.014	0.018		0.270
	Web	ASTM A36	35.84	54.63	31.58	Not Available					
HS-1A	Flange	ASTM A514	104.22	115.06	12.28	0.180	0.470	0.010	0.018	0.22	0.300
	Web	ASTM A36	49.02	60.83	19.09	0.100	0.440	0.010	0.024	0.22	0.060

TABLE 1.3 PHYSICAL AND CHEMICAL PROPERTIES OF COMPONENT PLATES

GIRDER	P_{crb} (kips)	P_{yw} (kips)	P_{yf} (kips)	P_p (kips)
	9.73	49.06	139.74	141.89
HB-2	12.03	51.04	141.51	143.74
HB-3	27.94	60.77	148.95	151.63
HB-4	31.79	38.67	94.20	95.53
HB-5	39.90	48.52	119.89	121.78

TABLE 1.4 REFERENCE LOADS FOR BENDING GIRDERS

GIRDER		P_{crs} (kips)	P_u (kips)	P_y (kips)
	T 1	30.12	91.81	189.46
HS1-A	T 2	44.37	133.21	189.46
	T 3	120.47	173.91	189.46

TABLE 1.5 REFERENCE LOADS FOR SHEAR GIRDER

GIRDER	$\beta^1 = \frac{h}{w}$	$\frac{b}{t}^1$	P_{ex} (kips)	$\frac{P_{ex}}{P_{yw}}$	$\frac{P_{ex}}{P_{yf}}$	$\frac{P_{ex}}{P_p}$	Mode of Failure
HB-1	305.1	7.95	129	2.63	0.92	0.91	V.B.[2]
HB-2	276.9	7.98	140	2.74	0.99	0.97	V.B.
HB-3	188.5	7.99	148	2.44	0.99	0.98	T.B.[3]
HB-4	145.8	15.54	55	1.42	0.58	0.57	T.B.
HB-5	145.8	10.85	80	1.65	0.67	0.66	T.B.

[1] Based on actual dimensions

[2] Vertical buckling of compression flange

[3] Torsional buckling of compression flange

TABLE 2.1 SUMMARY OF BENDING TESTS

GIRDER	TEST	$\beta^1 = \frac{h}{w}$	$\alpha = \frac{a}{h}$	P_{ex} (kips)	$\frac{P_{ex}}{P_{crs}}$	$\frac{P_{ex}}{P_y}$	$\frac{P_{ex}}{P_u}$
HS-1A	T-1	192.2	2.0	98	3.25	0.52	1.07
	T-2	192.2	1.0	125	2.82	0.66	0.94
	T-3	192.2	0.5	167	1.39	0.88	0.96

[1] Based on actual dimensions

TABLE 3.1 SUMMARY OF SHEAR TESTS

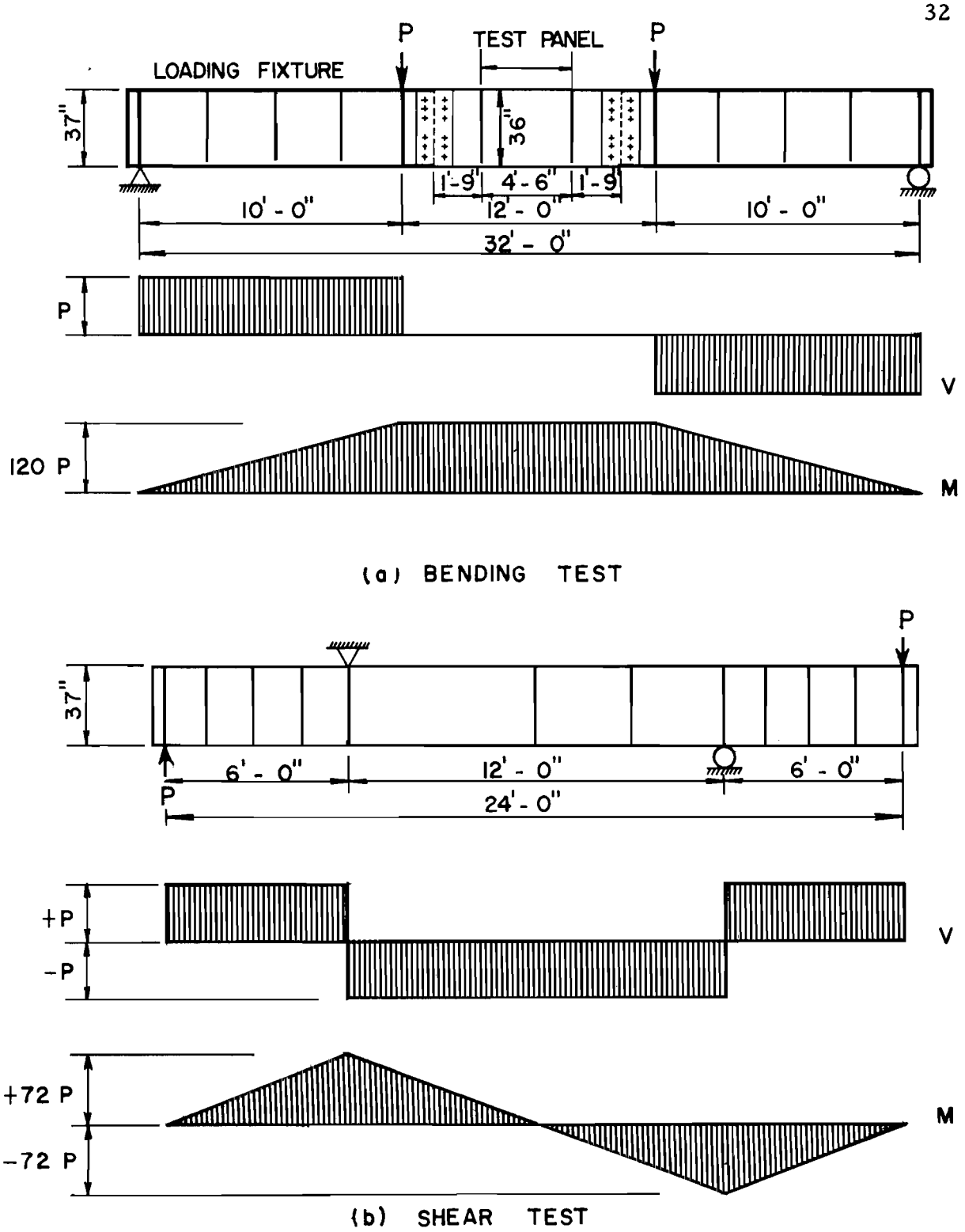

Fig. 1.1 Loading Condition of Bending and Shear Test

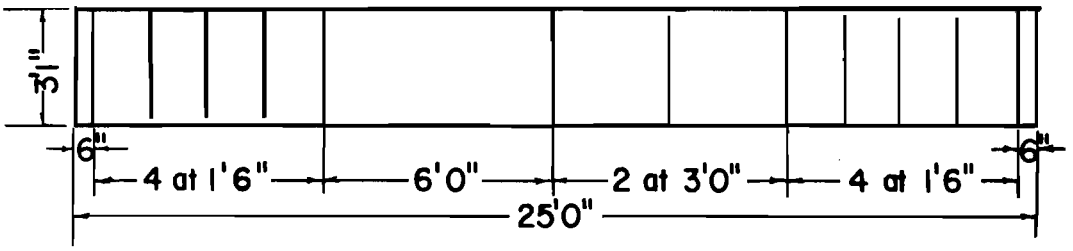

(a) TEST 1, (72-inch panels)

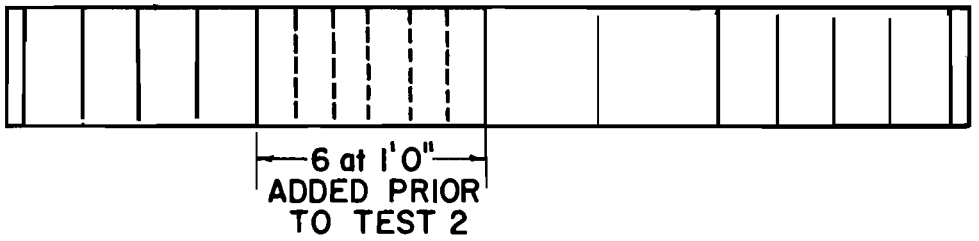

(b) TEST 2, (36-inch panels)

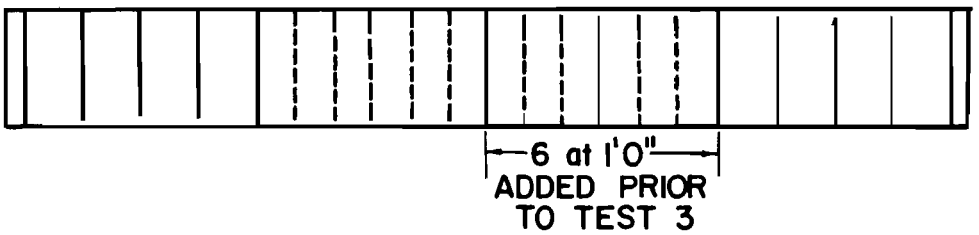

(c) TEST 3, (18-inch panels)

Fig. 1.2 Arrangement of Repair Stiffeners and Test Sequence

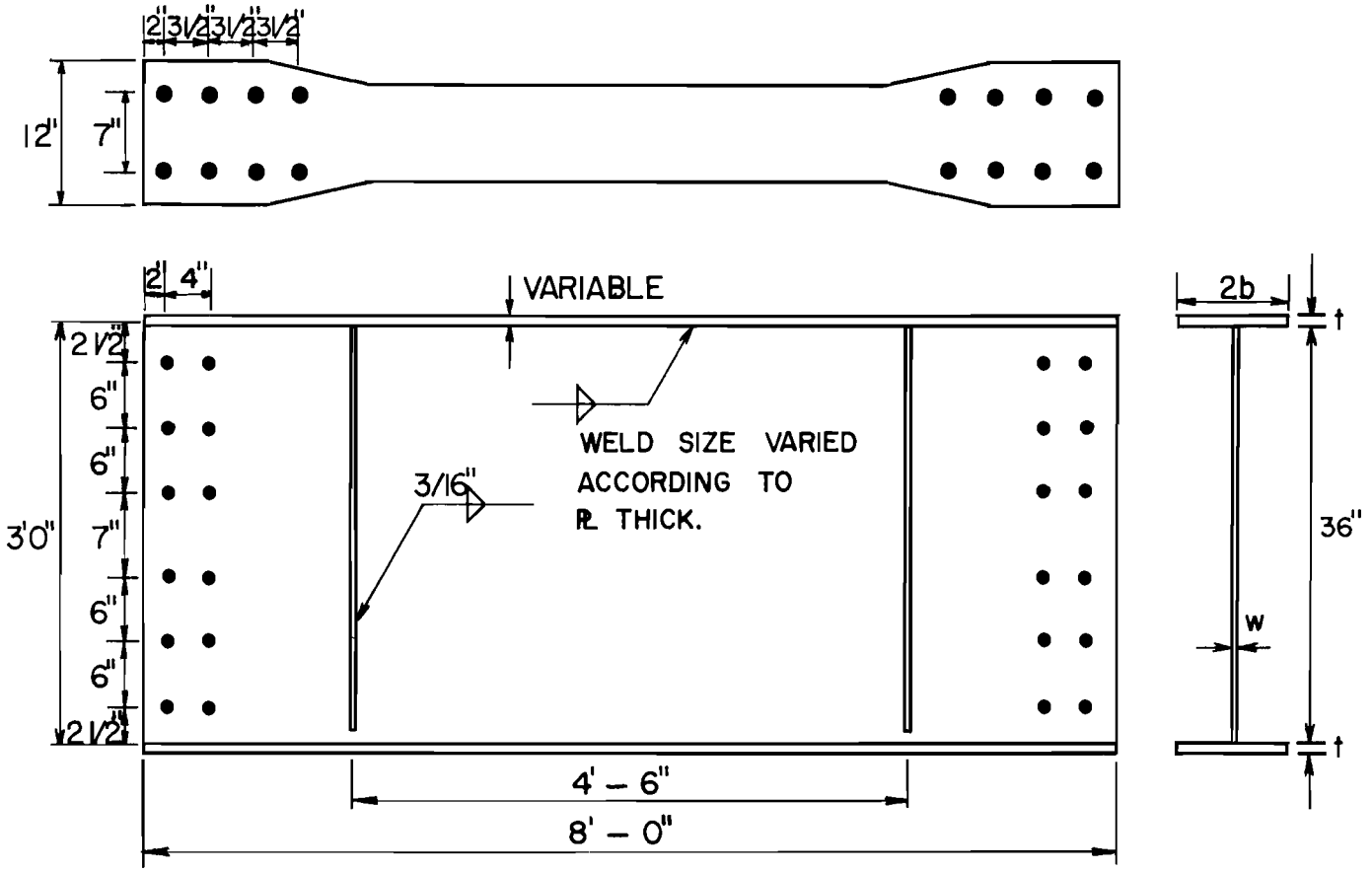

GIRDER	2 b (in.)	t (in.)	w (in.)
HB – 1	8	1/2	11 GA.
HB – 2	8	1/2	10 GA.
HB – 3	8	1/2	3/16
HB – 4	8	1/4	1/4
HB – 5	8	3/8	1/4

Fig. 1.3 Test Girders HB-1 to HB-5

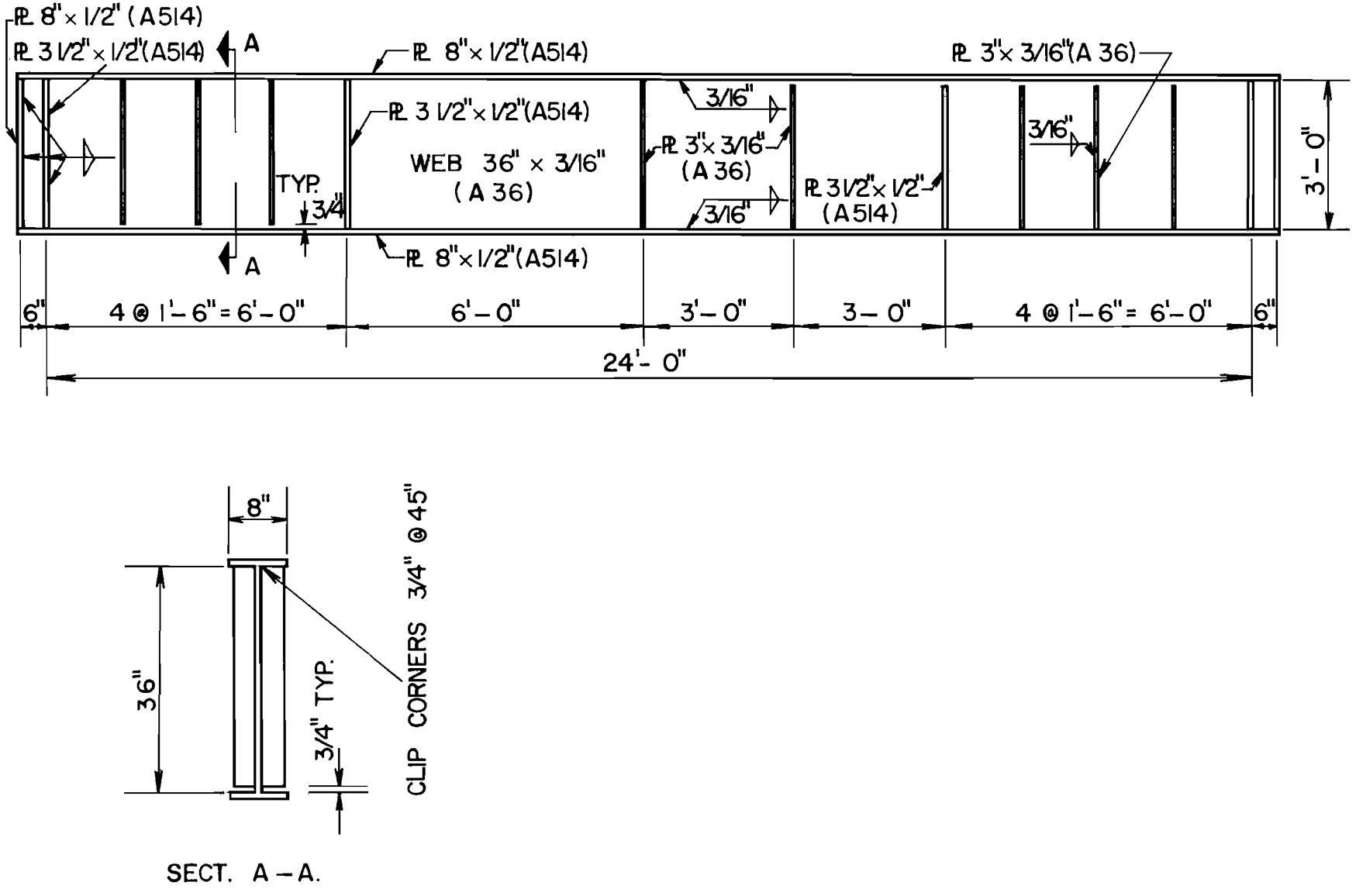

Fig. 1.4 Test Girder HS-1A

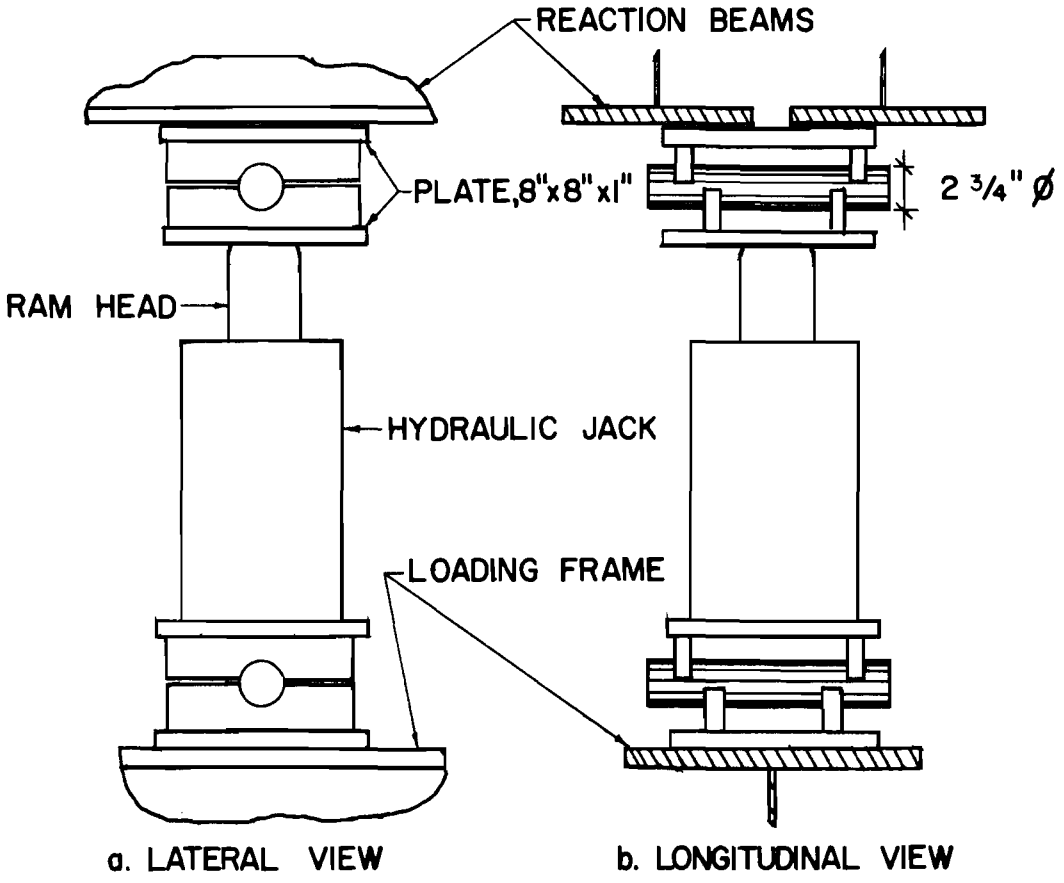

Fig. 2.1 Loading System

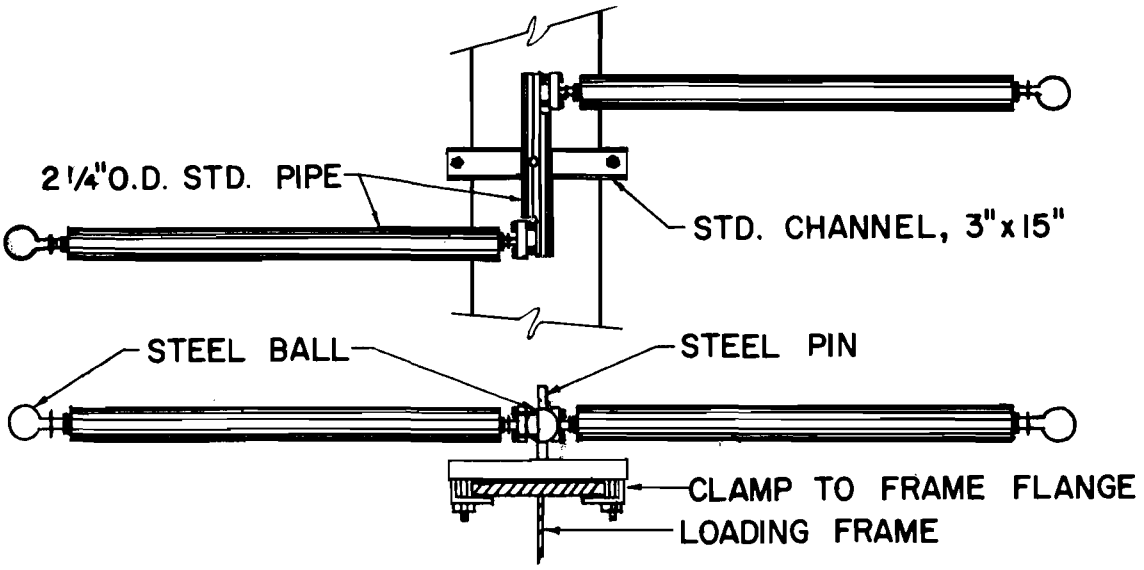

Fig. 2.2 Lateral Support System

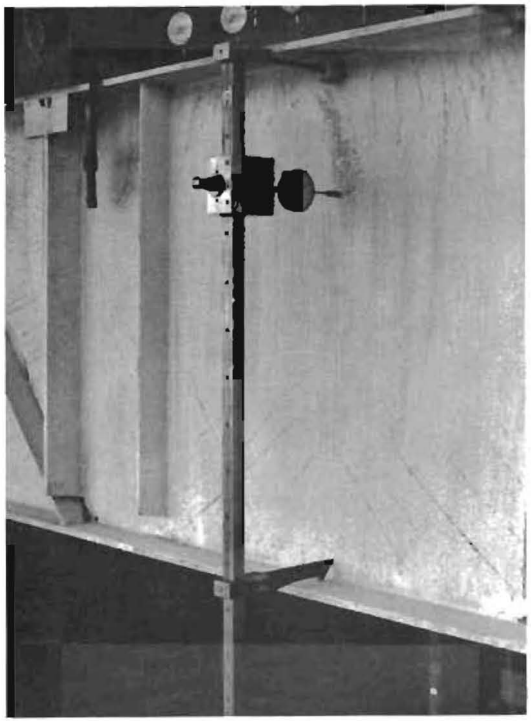

Fig. 2.3 Movable Head Dial Rig Used to Measure Web Deflections

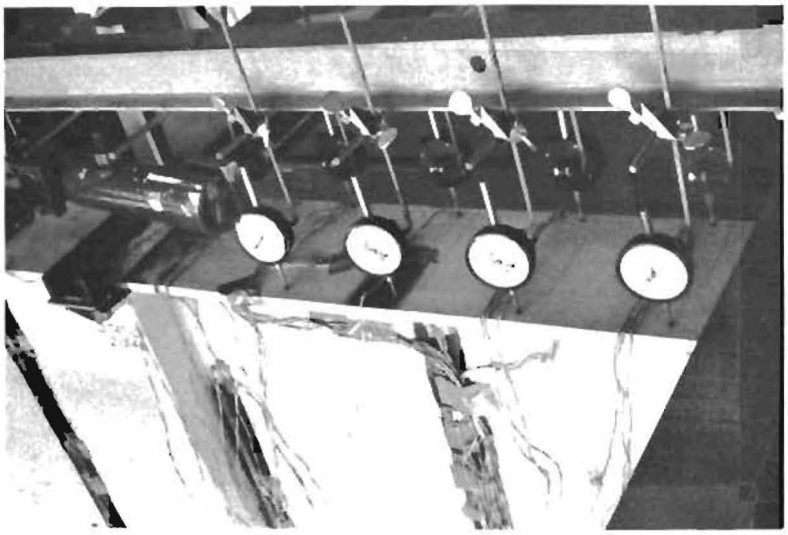

Fig. 2.4 Dial Gages Used to Measure Compression Flange Rotation

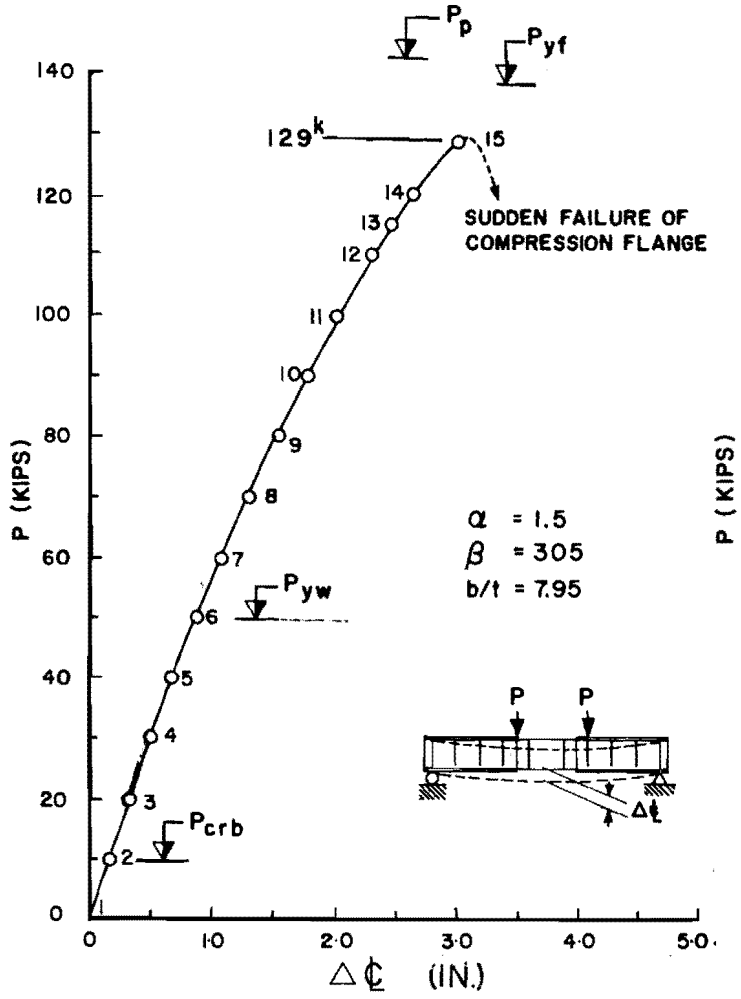

Fig. 2.5 Load vs. Deflection Curve for Girder HB-1

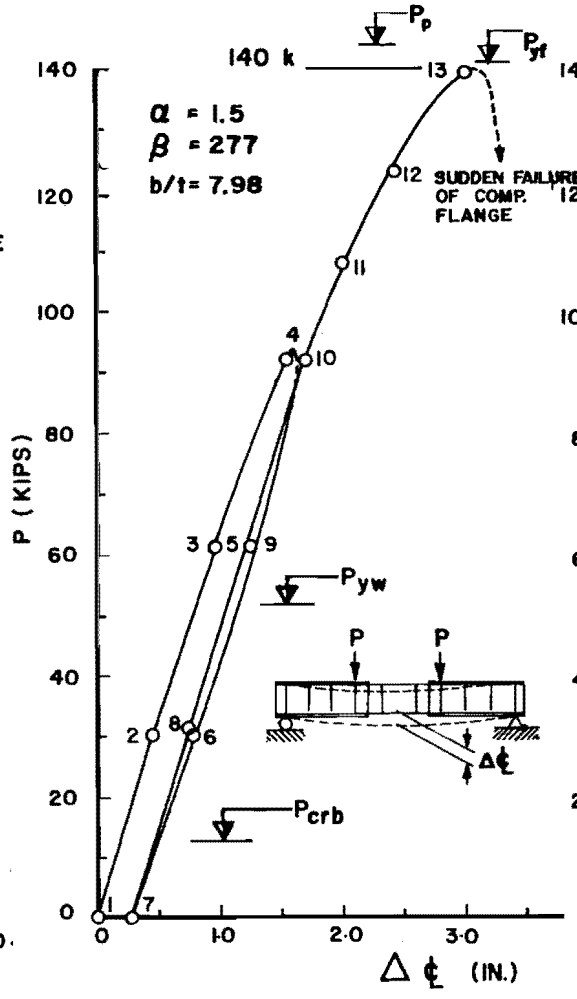

Fig. 2.6 Load vs. Deflection Curve for Girder HB-2

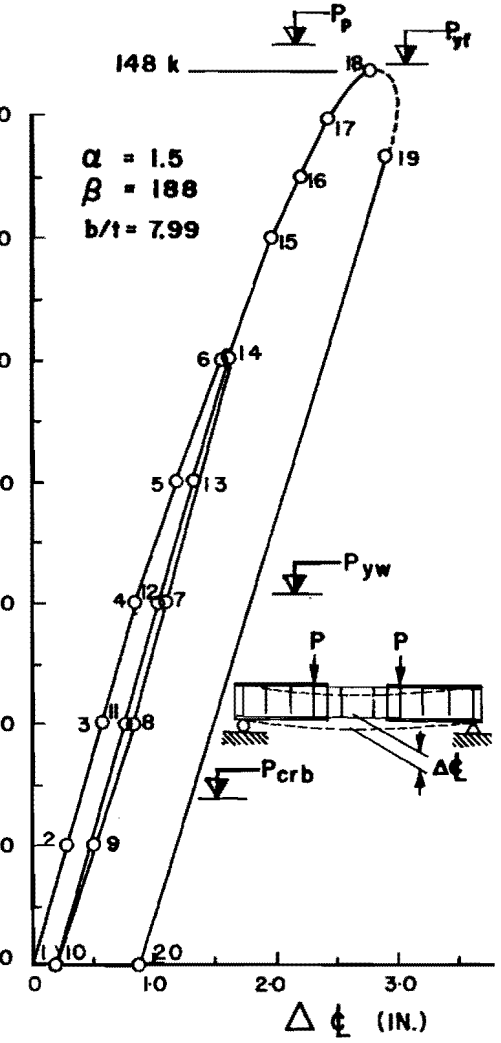

Fig. 2.7 Load vs. Deflection Curve for Girder HB-3

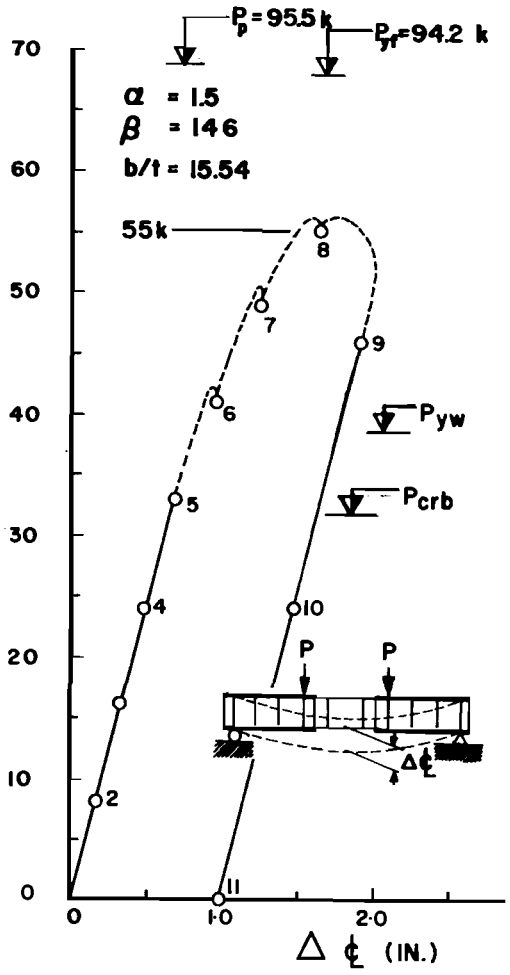

Fig. 2.8 Load vs. Deflection Curve for Girder HB-4

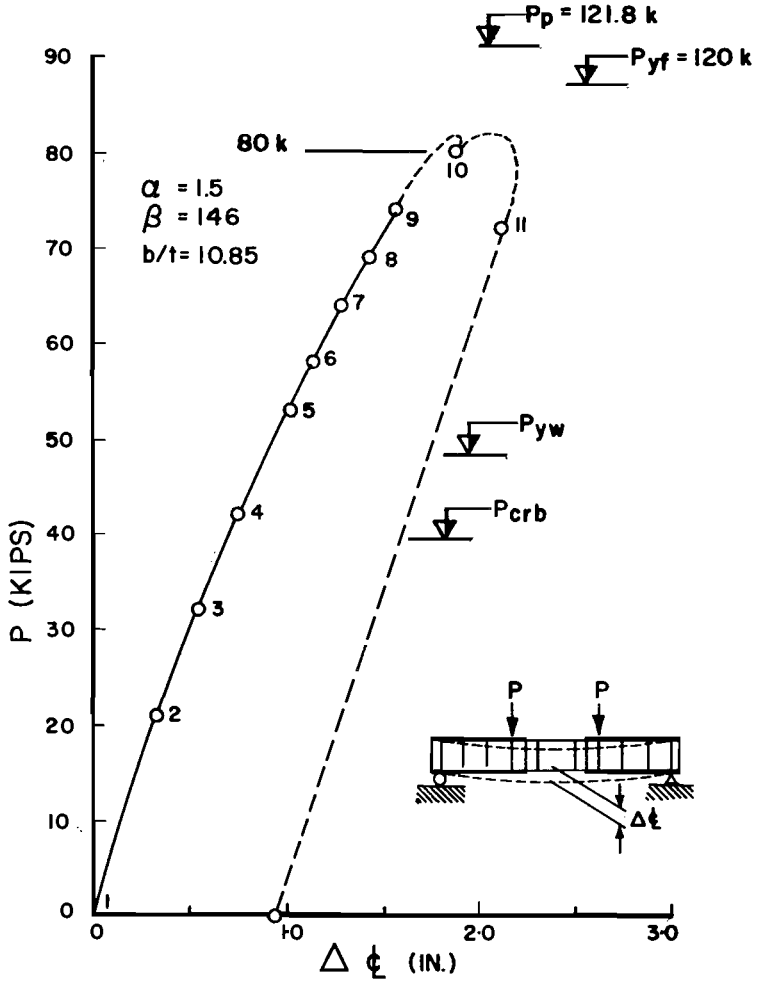

Fig. 2.9 Load vs. Deflection Curve for Girder HB-5

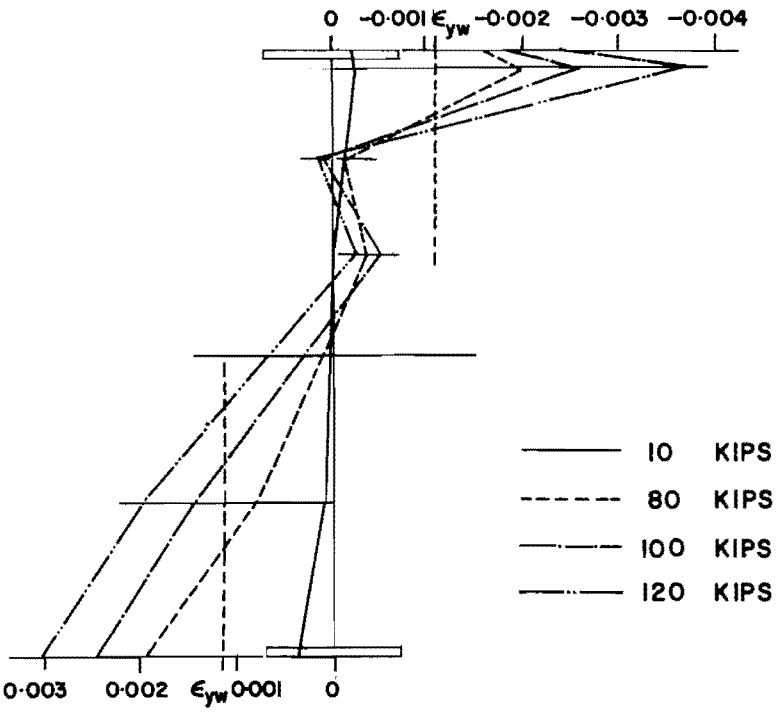

Fig. 2.10 Bending Strain Distribution Girder HB-1

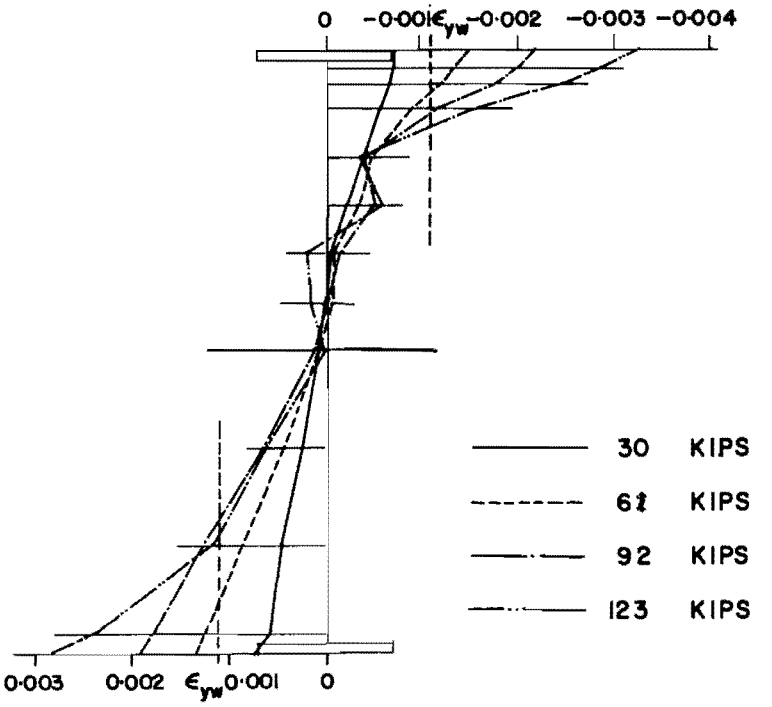

Fig. 2.11 Bending Strain Distribution Girder HB-2

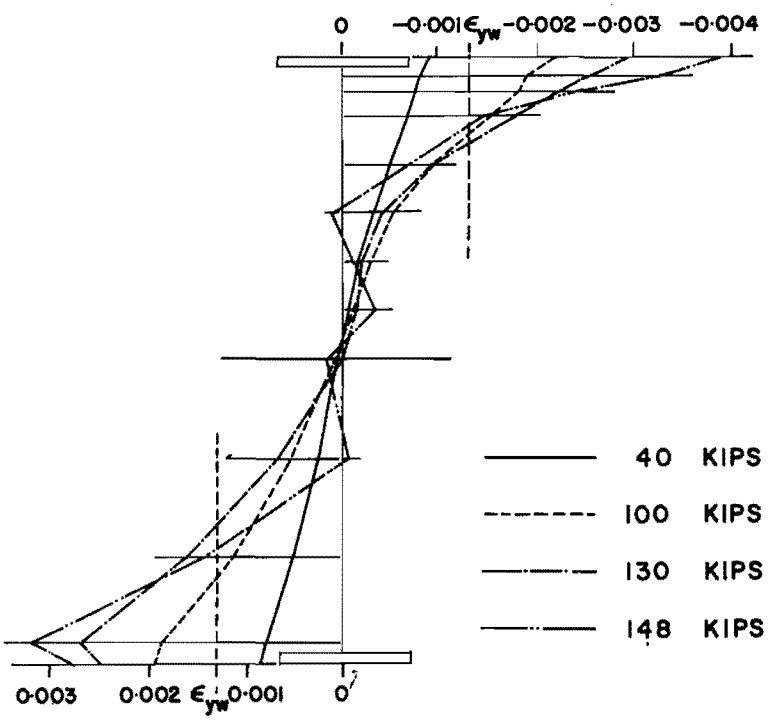

Fig. 2.12 Bending Strain Distribution Girder HB-3

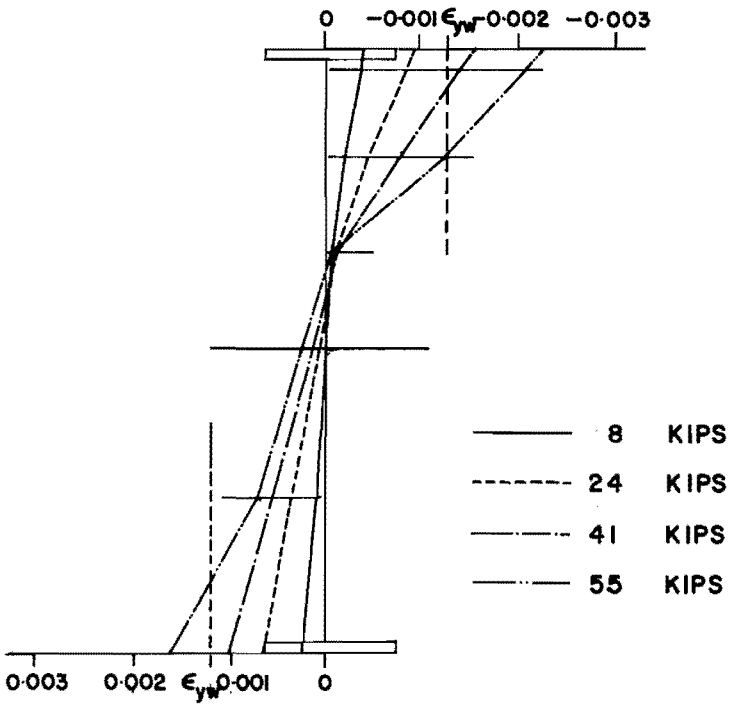

Fig. 2.13 Bending Strain Distribution Girder HB-4

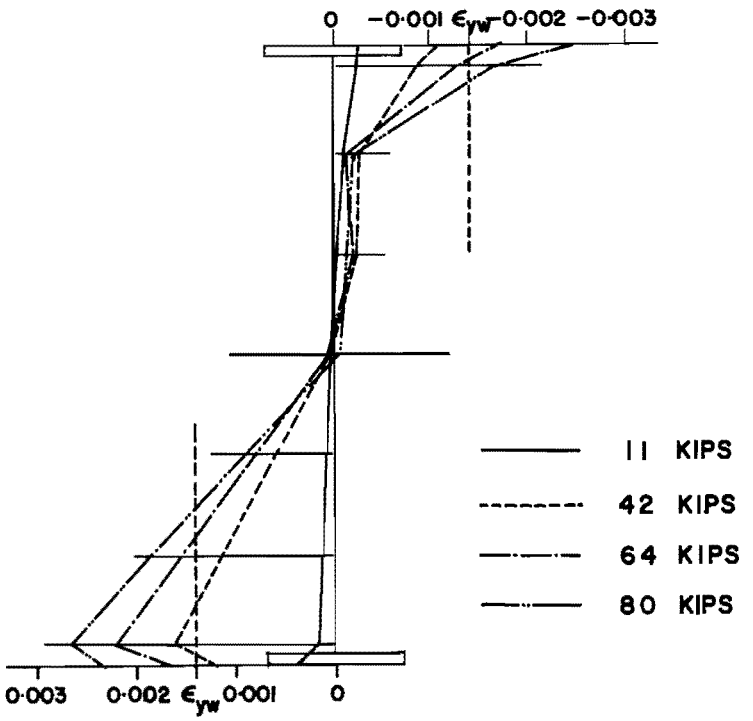

Fig. 2.14 Bending Strain Distribution Girder HB-5

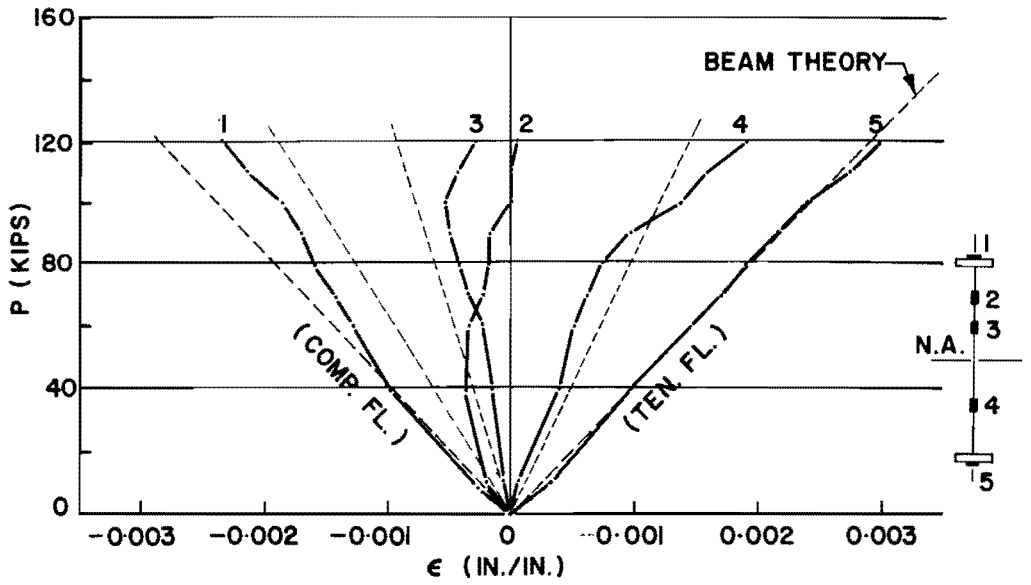

Fig. 2.15 P - ϵ Curve, Girder HB-1

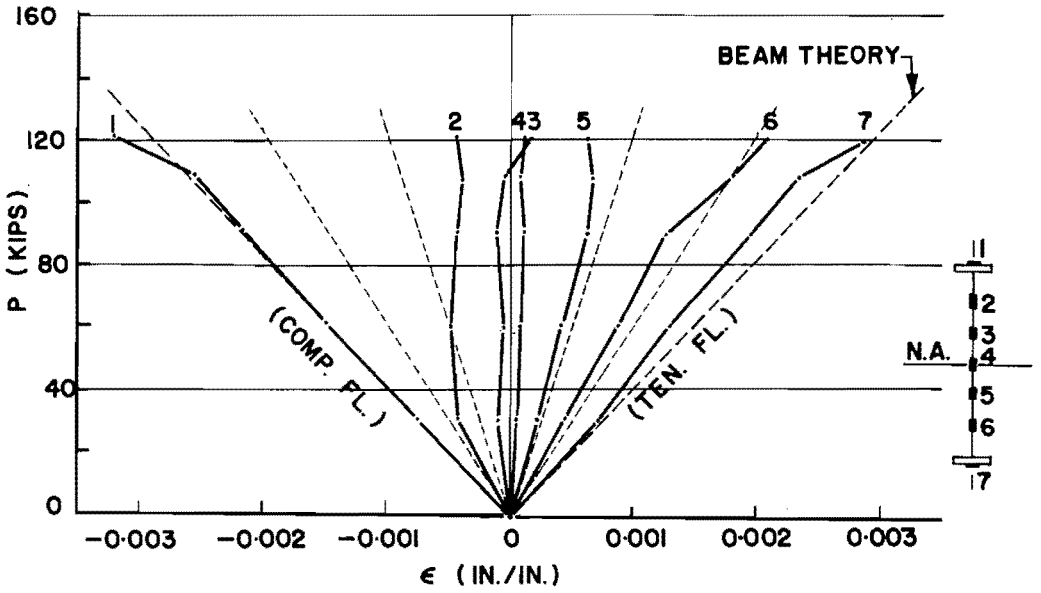

Fig. 2.16 P - ϵ Curve,Girder HB-2

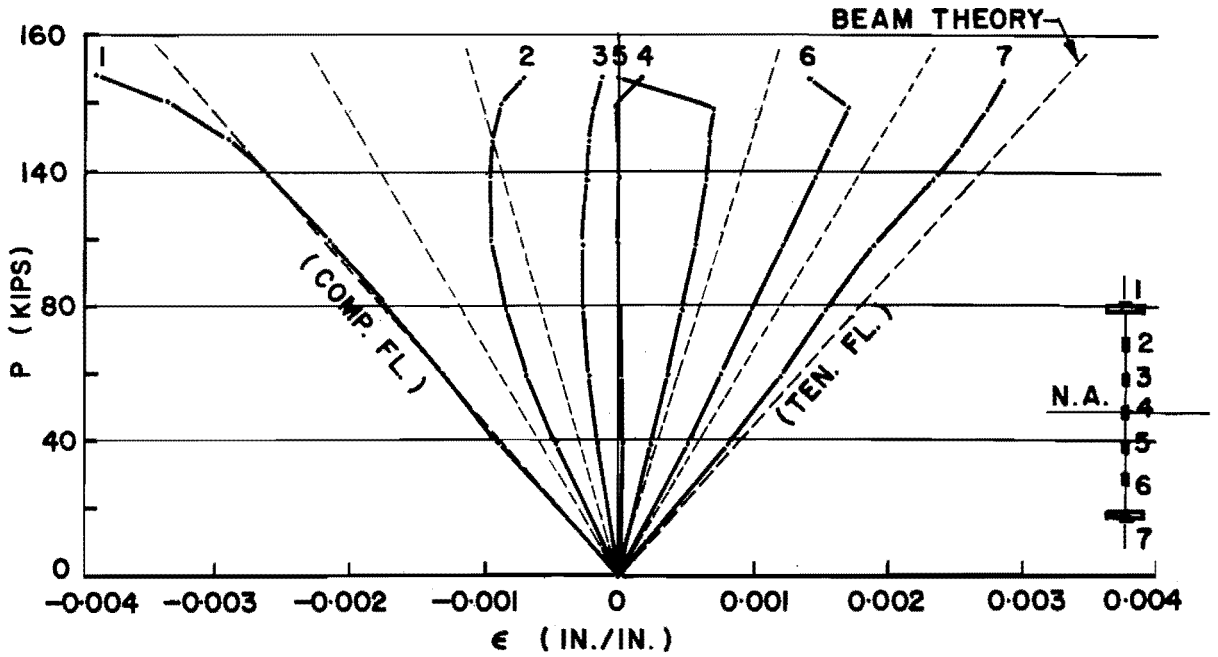

Fig. 2.17 P - ϵ Curve,Girder HB-3

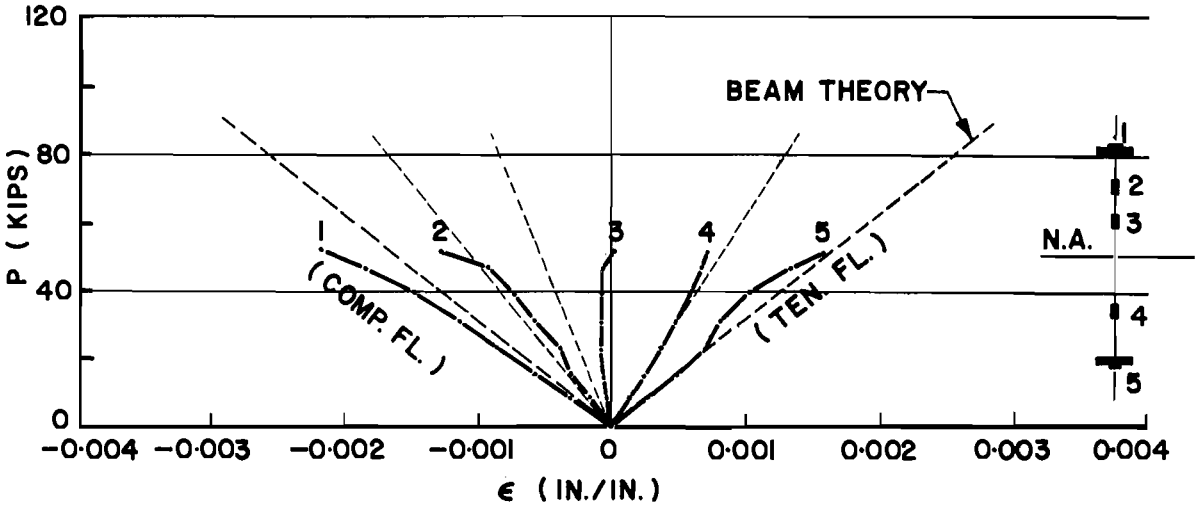

Fig. 2.18 P - ϵ Curve, Girder HB-4

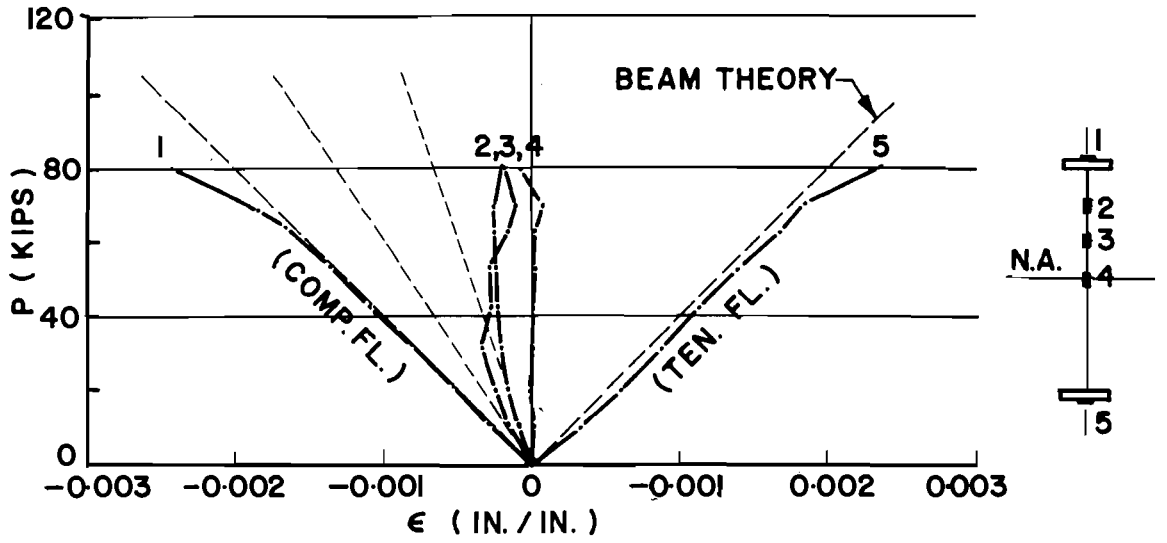

Fig. 2.19 P - ϵ Curve, Girder HB-5

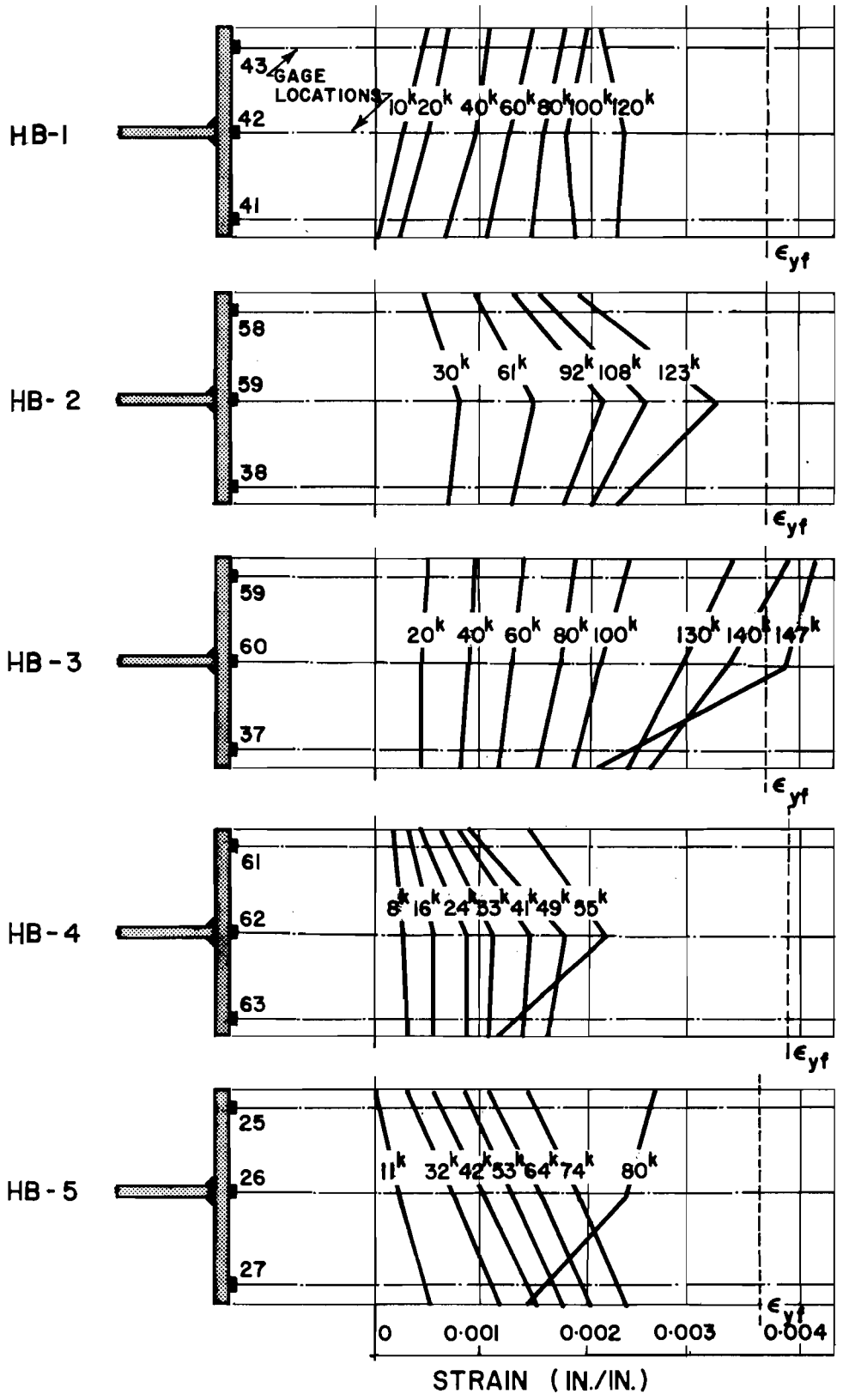

Fig. 2.20 Compression Flange Strain Distribution

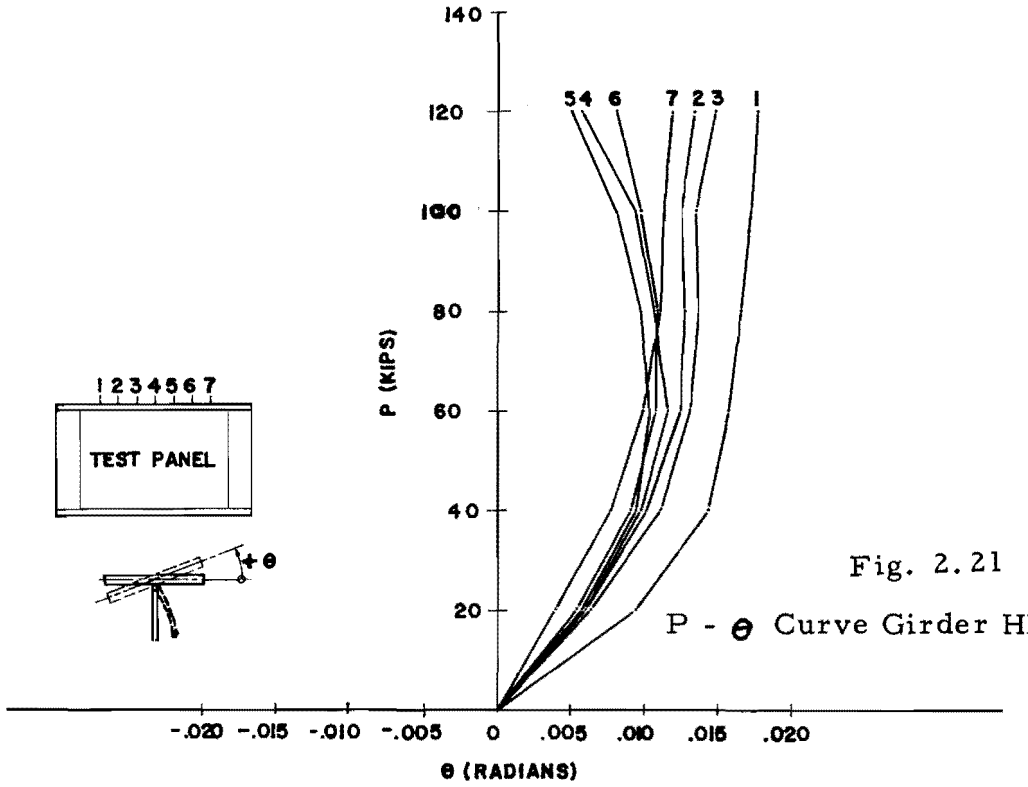

Fig. 2.21

P - θ Curve Girder HB-1

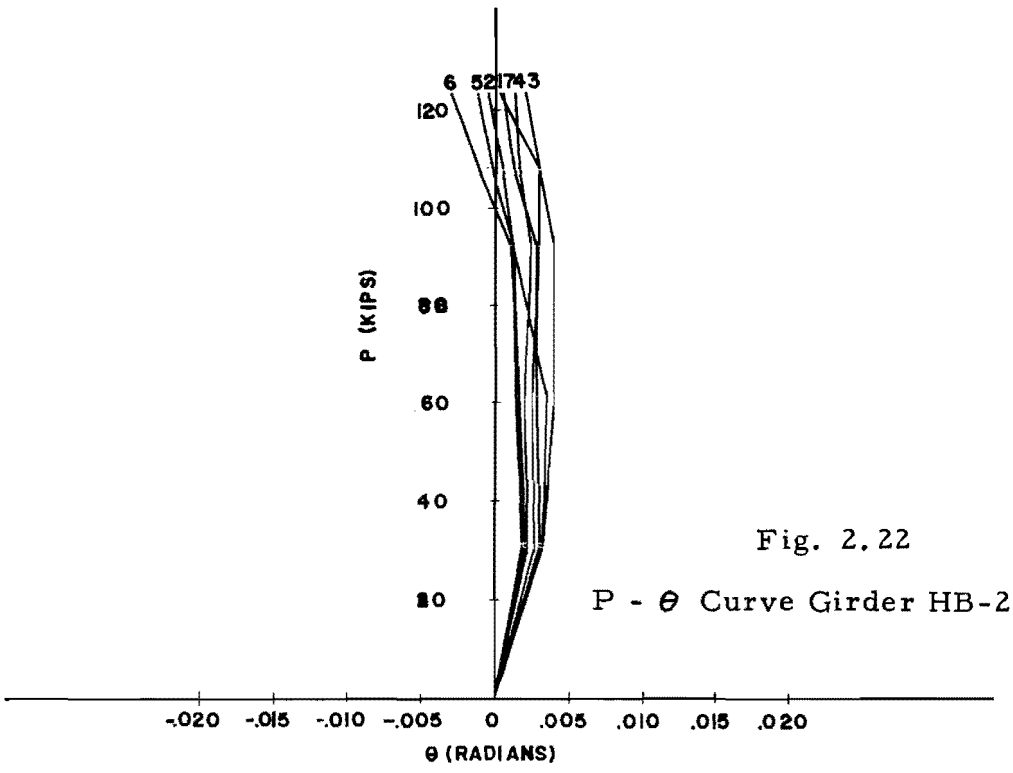

Fig. 2.22

P - θ Curve Girder HB-2

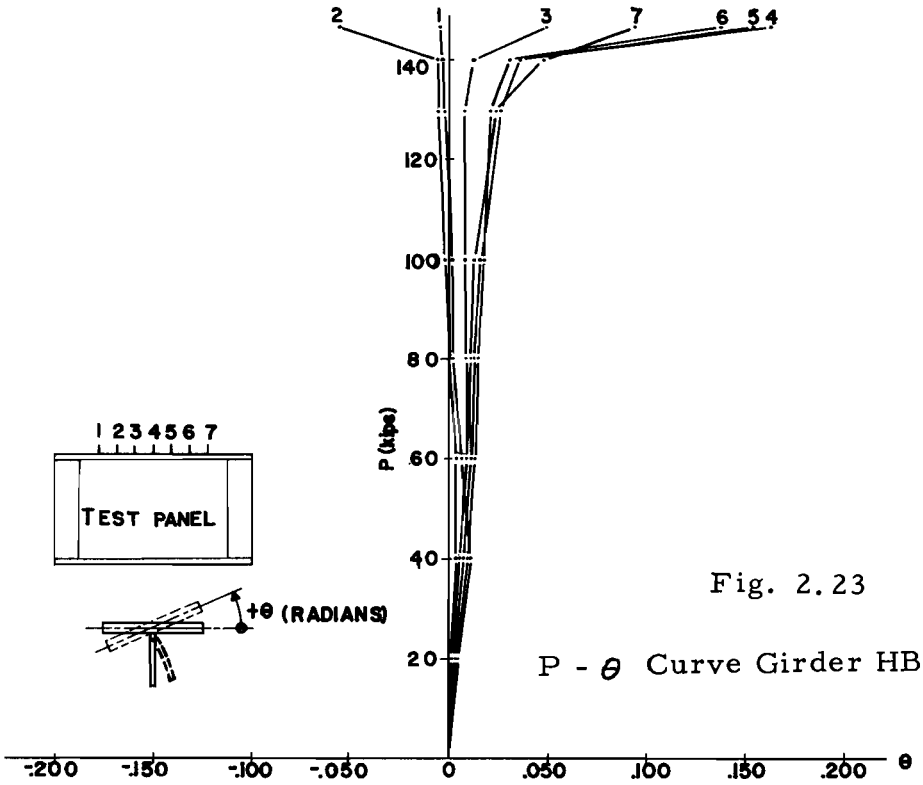

Fig. 2.23

P - θ Curve Girder HB-3

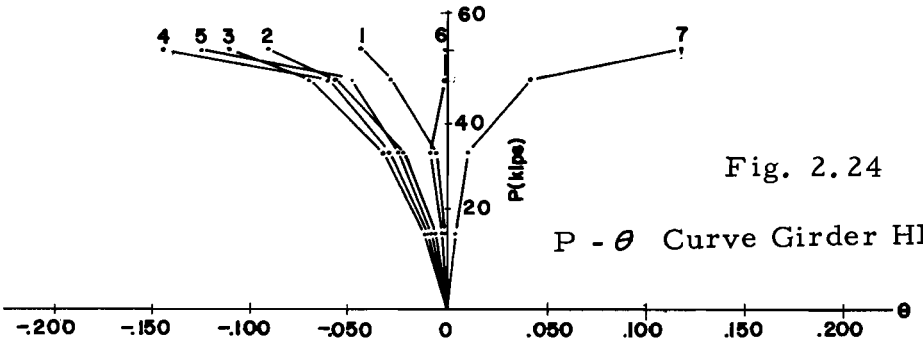

Fig. 2.24

P - θ Curve Girder HB-4

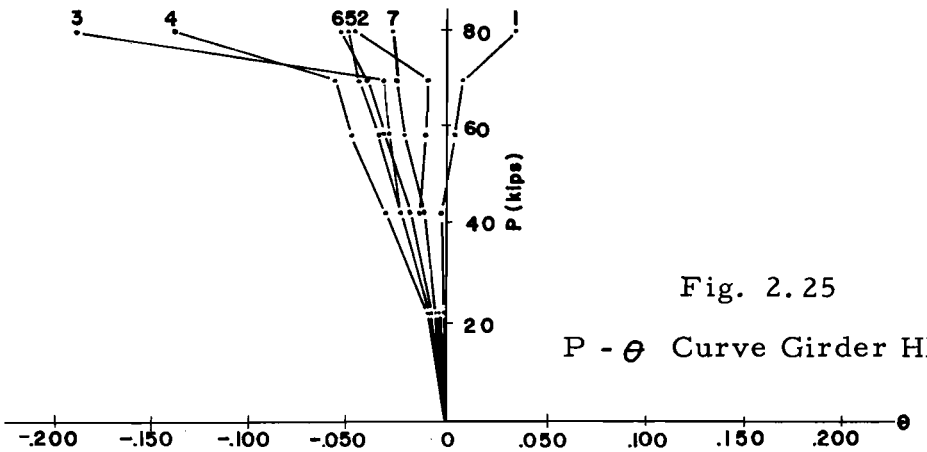

Fig. 2.25

P - θ Curve Girder HB-5

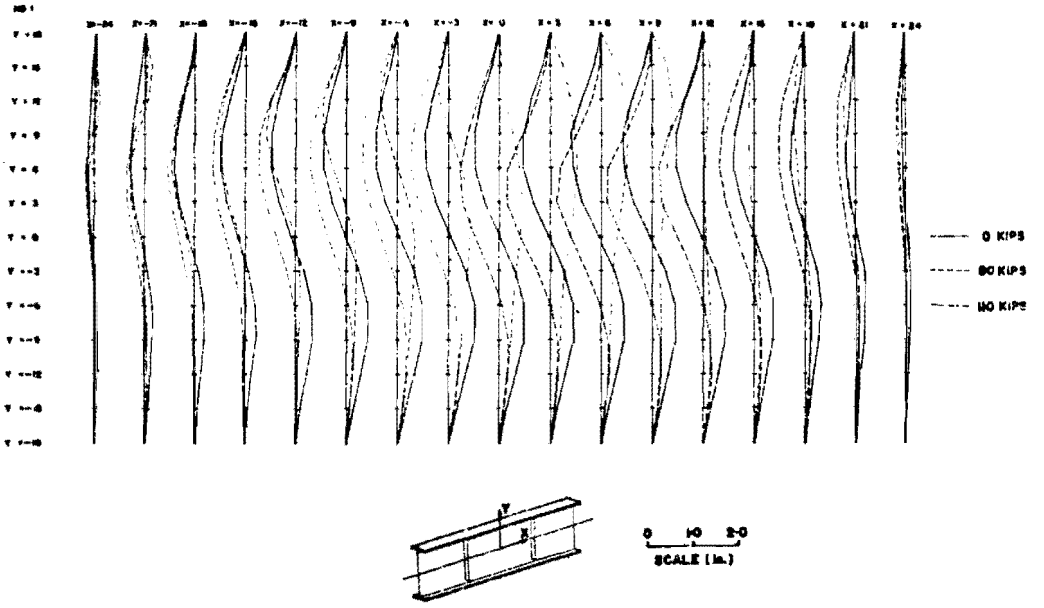

Fig. 2.26 Web Deflections of Girder HB-1

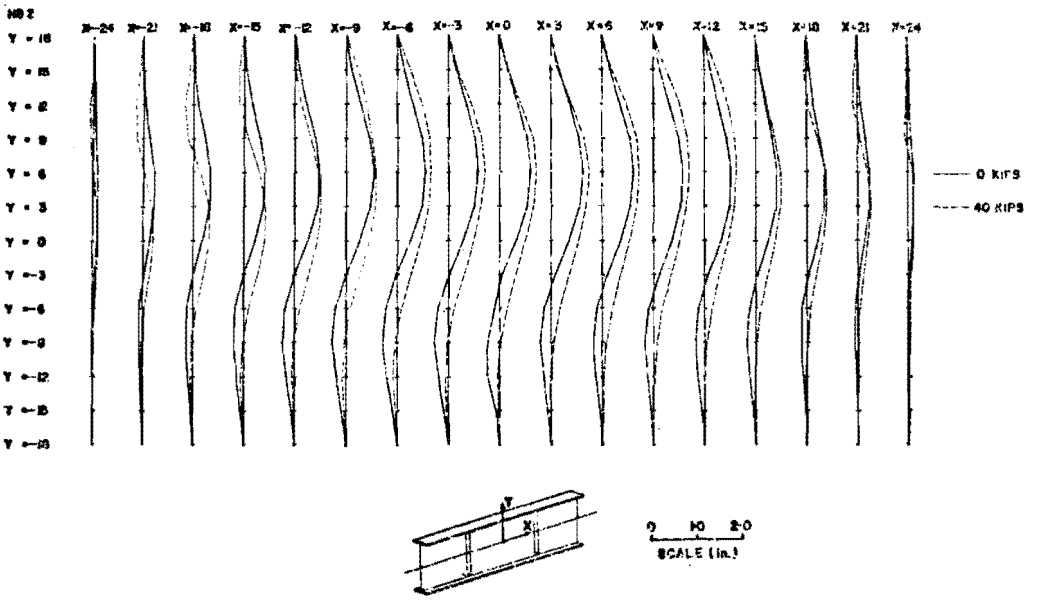

Fig. 2.27 Web Deflections of Girder HB-2

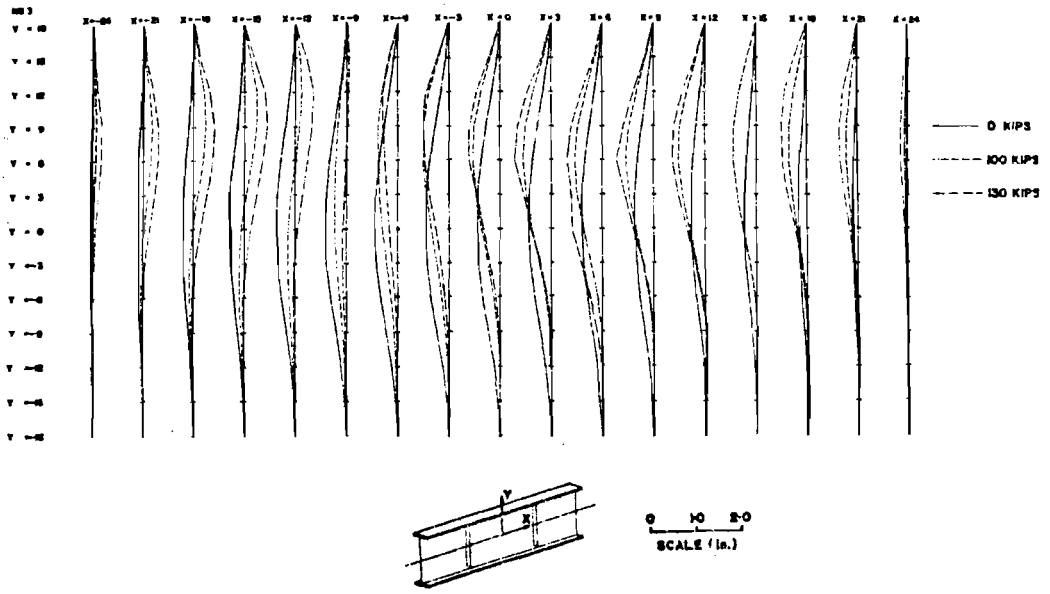

Fig. 2.28 Web Deflections of Girder HB-3

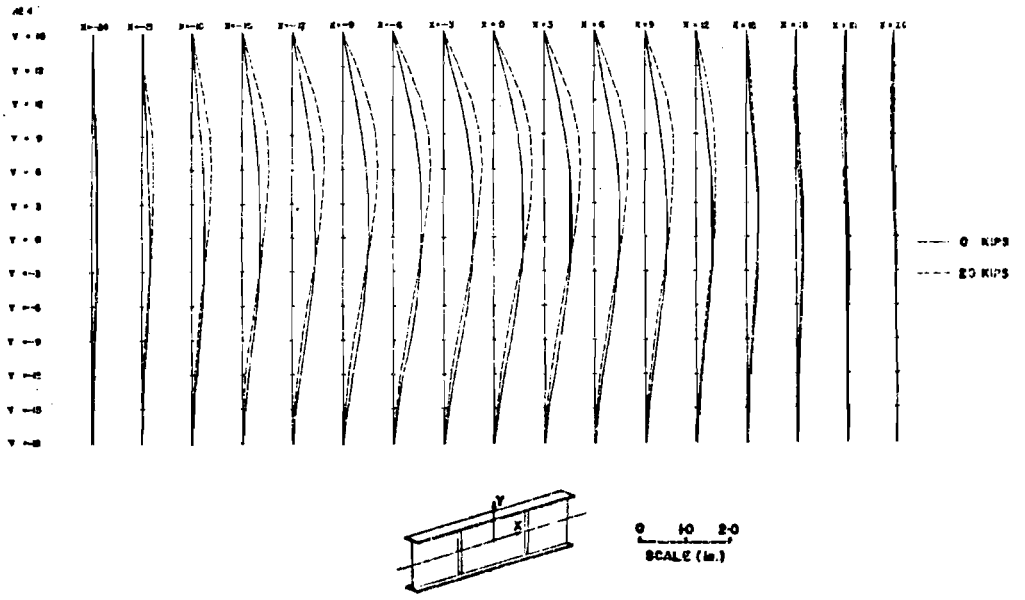

Fig. 2.29 Web Deflections of Girder HB-4

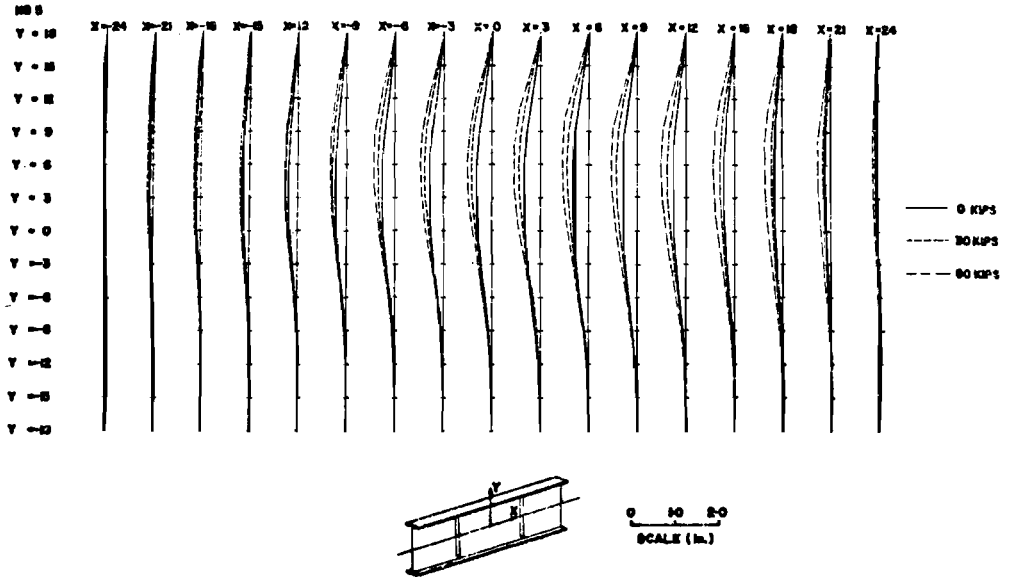

Fig. 2.30 Web Deflections of Girder HB-5

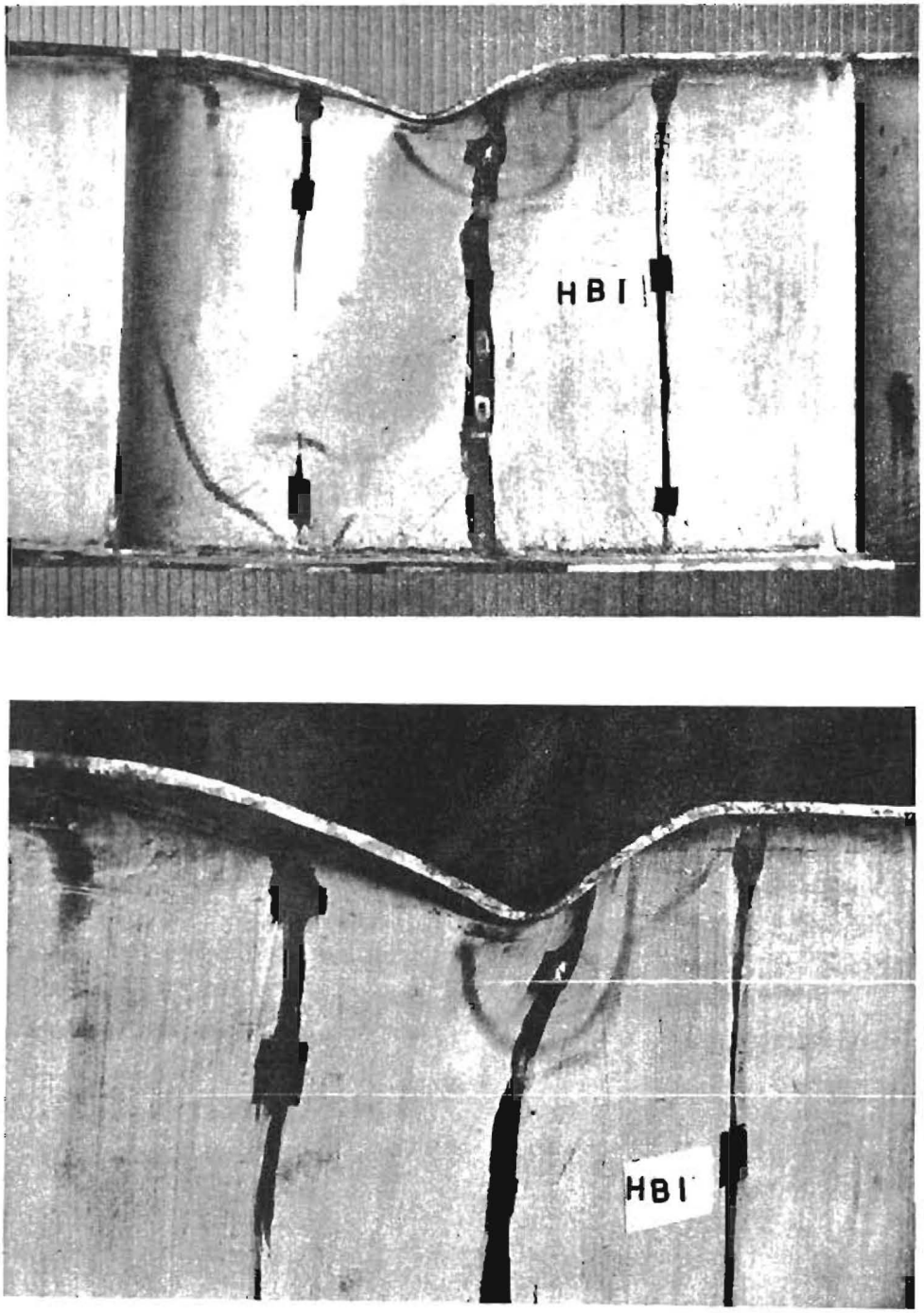

Fig. 2.31 Girder HB-1 after Test

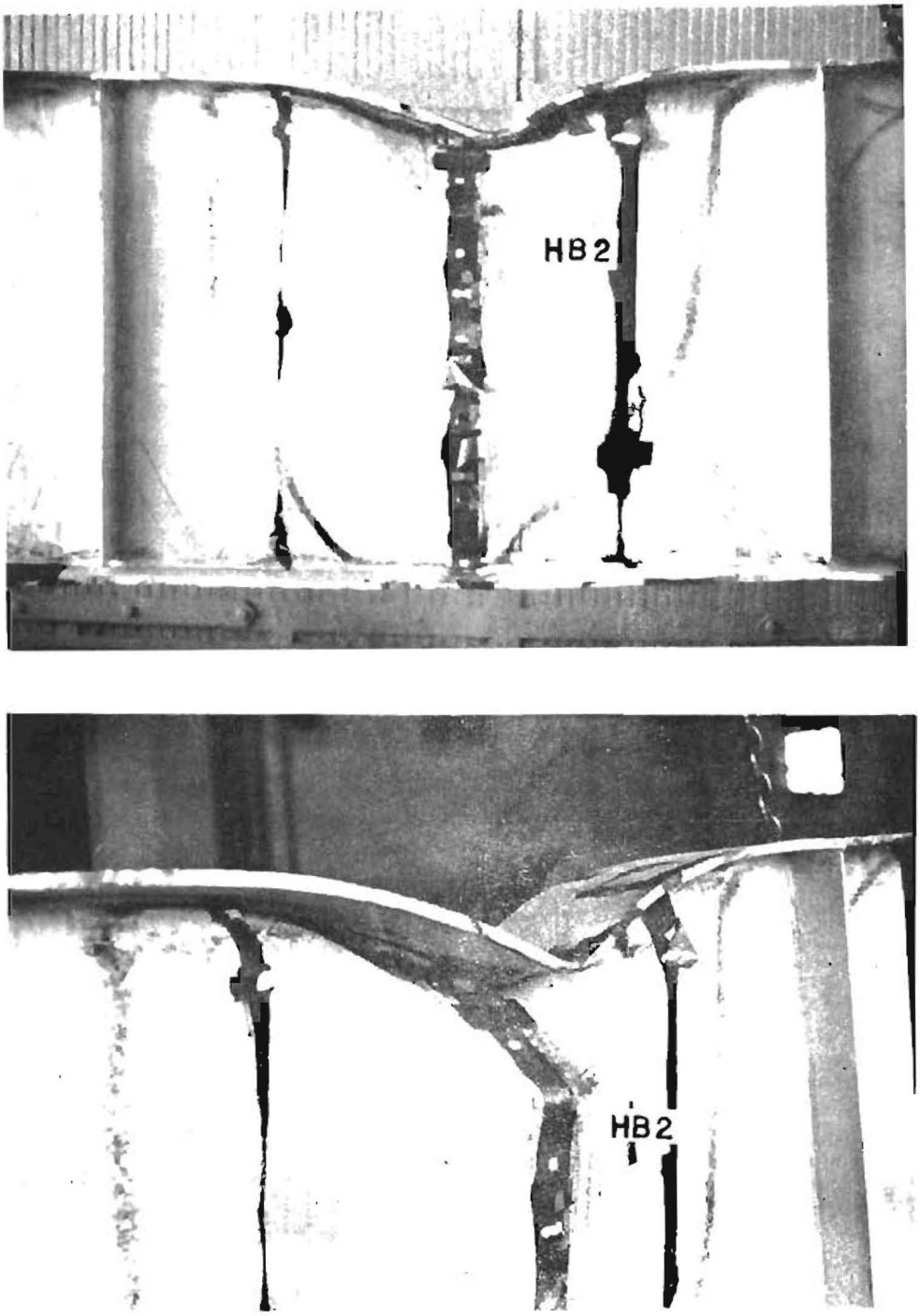

Fig. 2.32 Girder HB-2 after Test

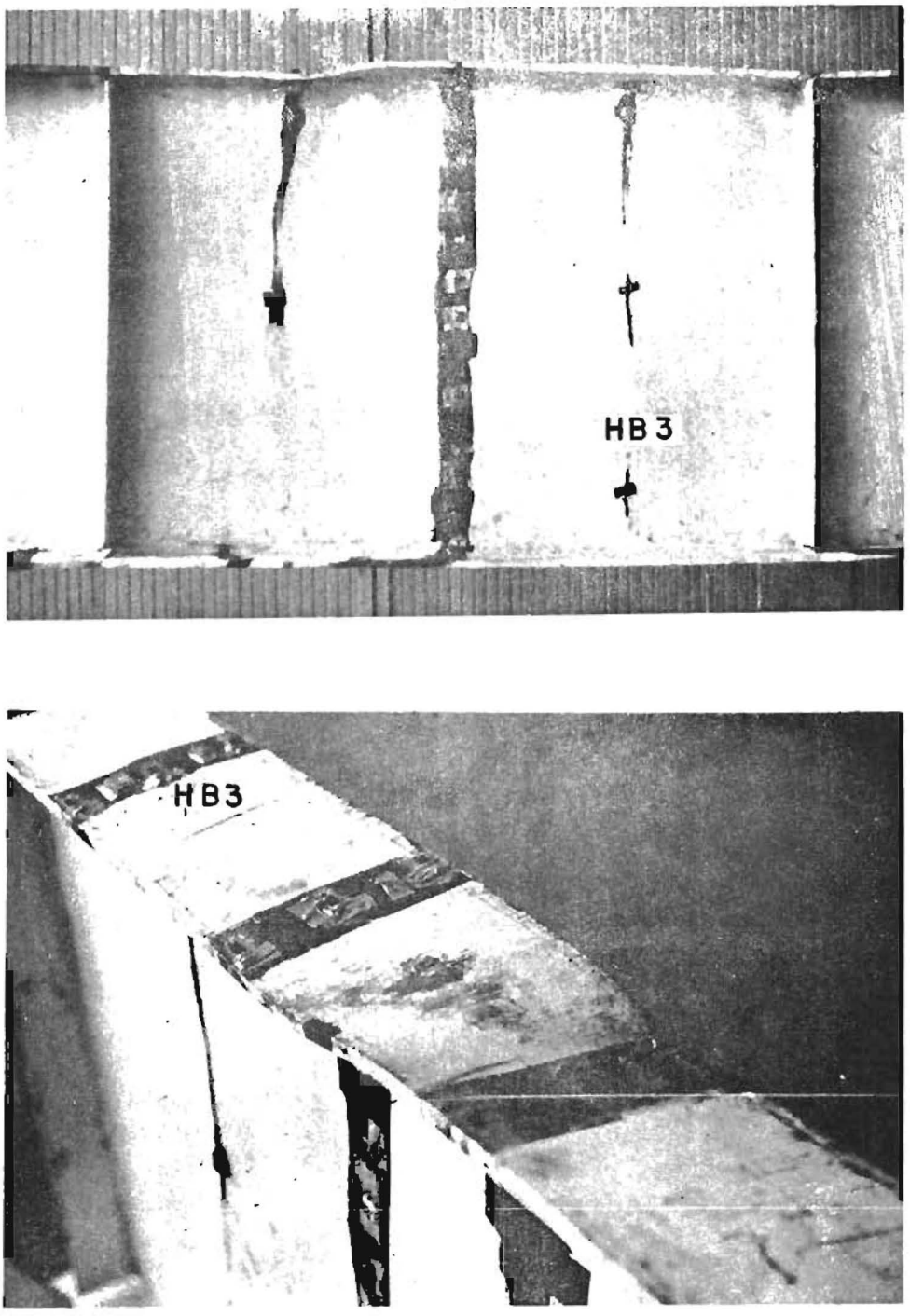

Fig. 2.33 Girder HB-3 after Test

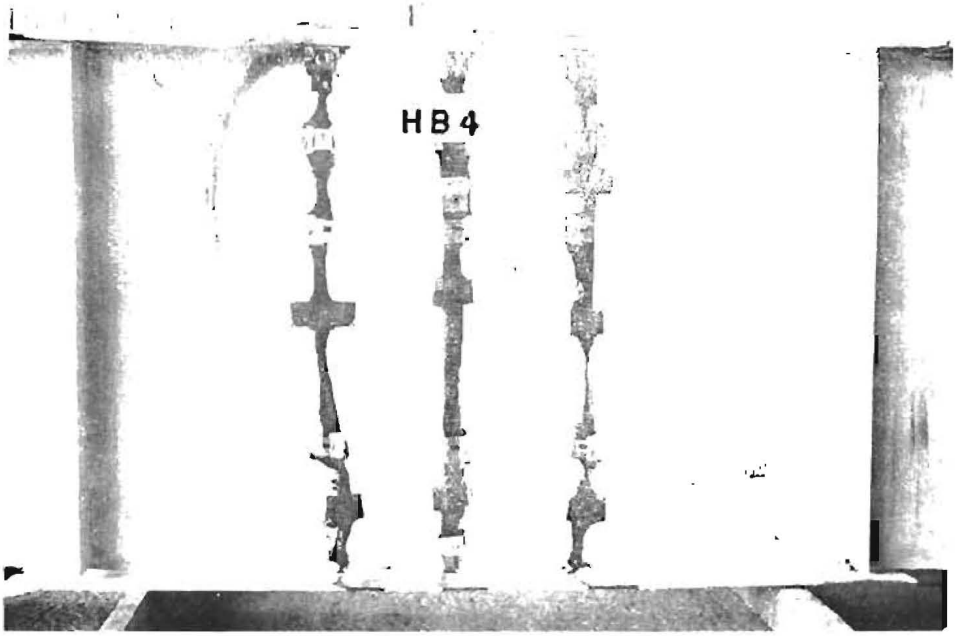

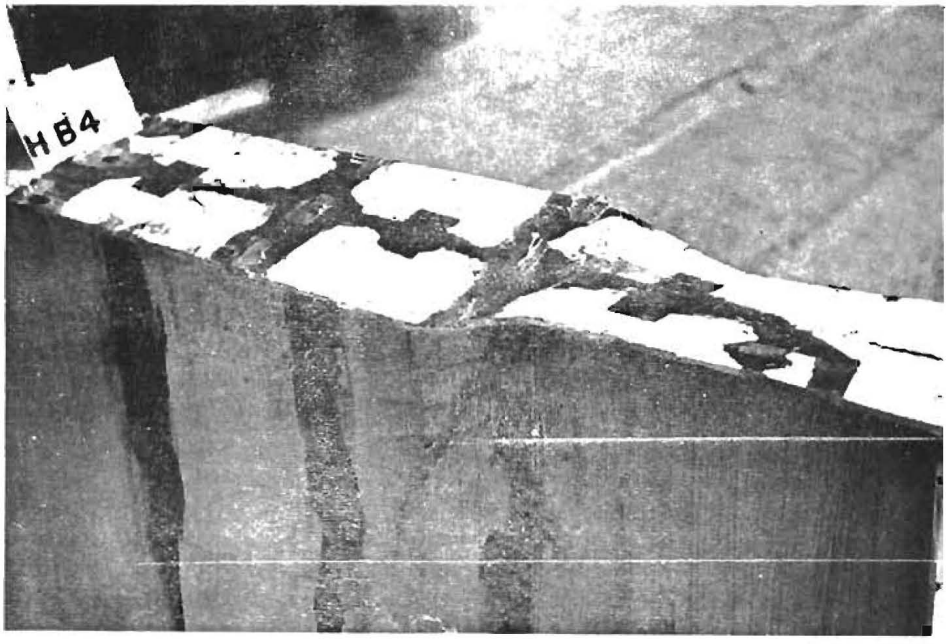

Fig. 2.34 Girder HB-4 after Test

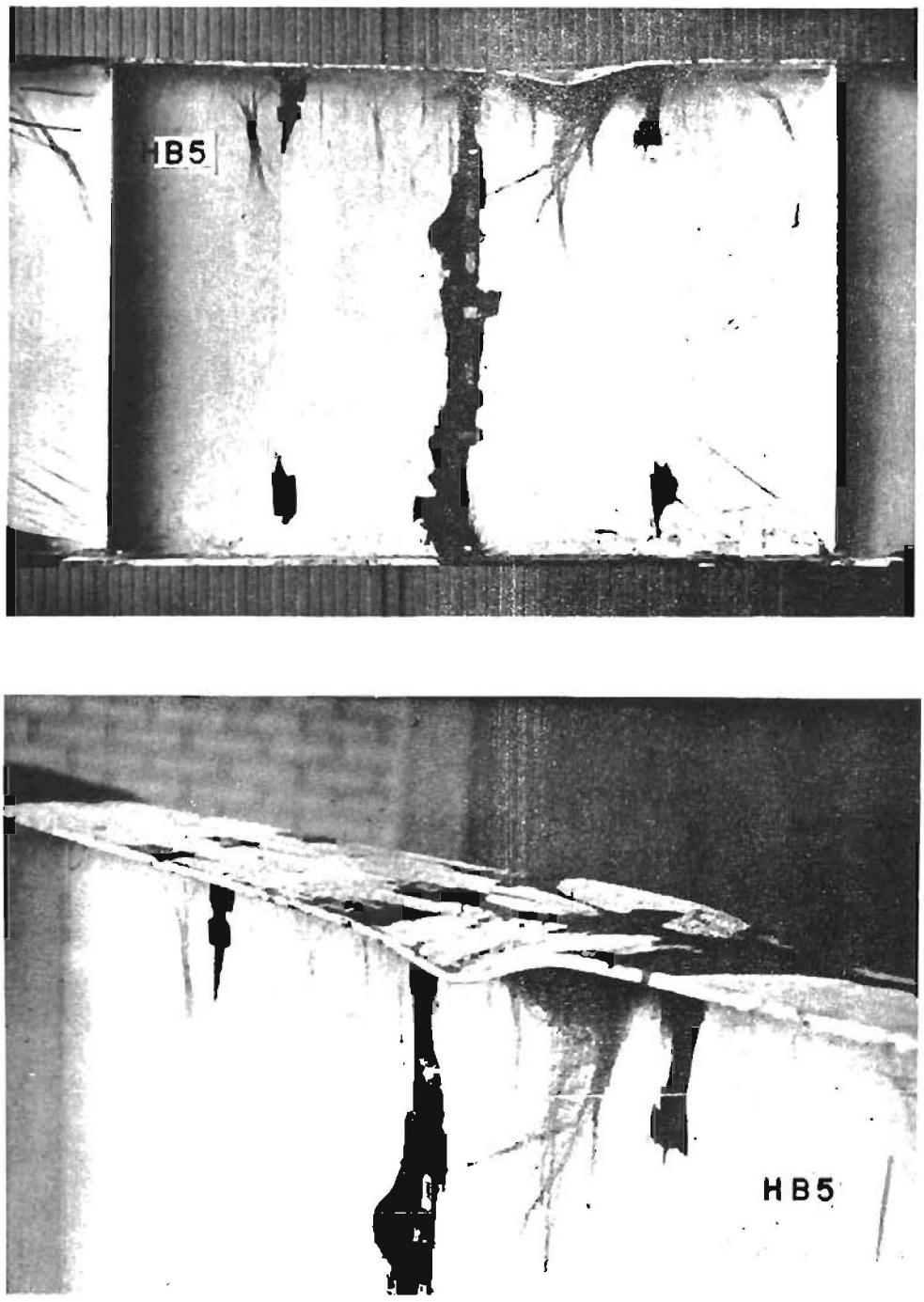

Fig. 2.35 Girder HB-5 after Test

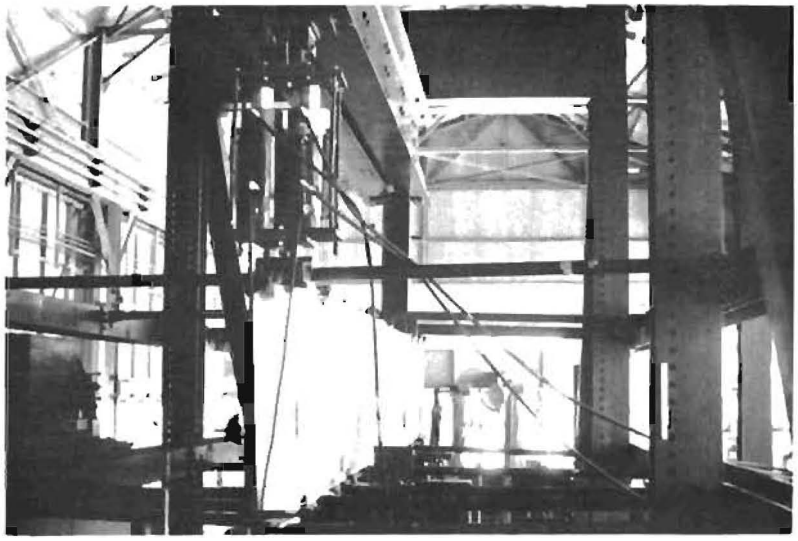

Fig. 3.1 Overall View of Test Setup

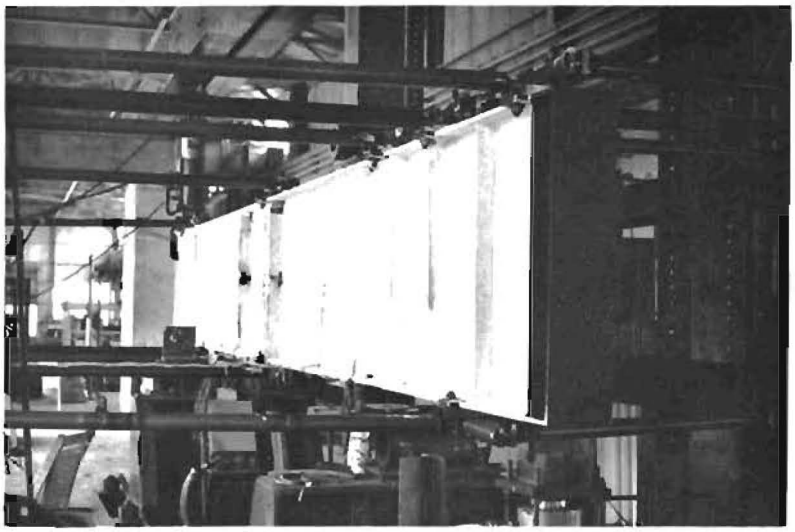

Fig. 3.2 Lateral Support System

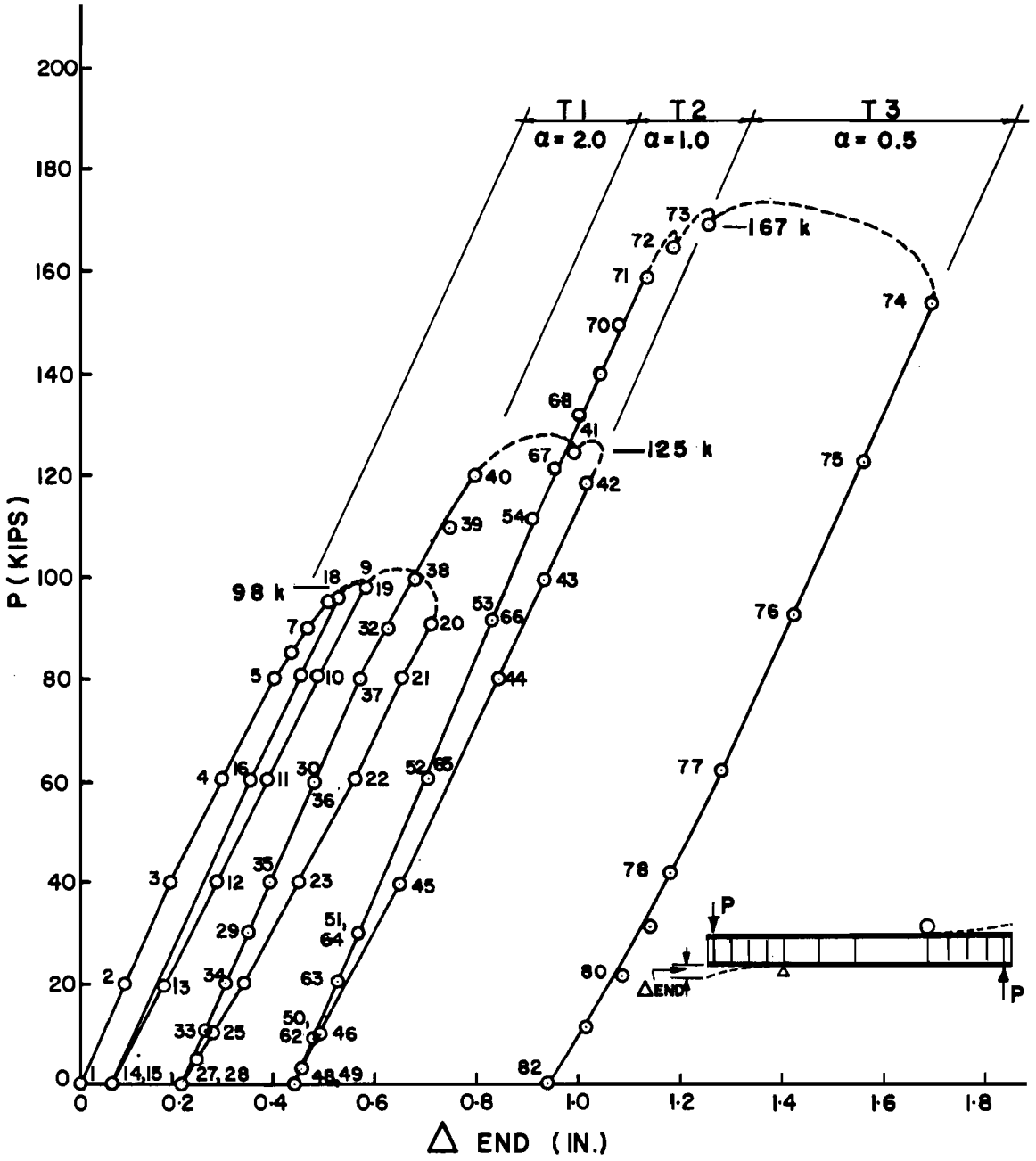

Fig. 3.3 Load vs. Deflection Curves for Girder HS-1A, T1, T2 and T3

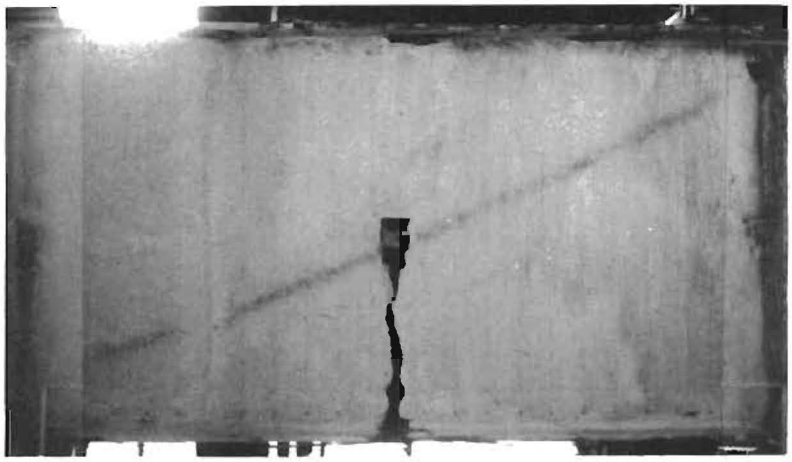

Fig. 3.4 Mode of Failure of $\alpha = 2.0$
Panel Girder HS-1A, T1

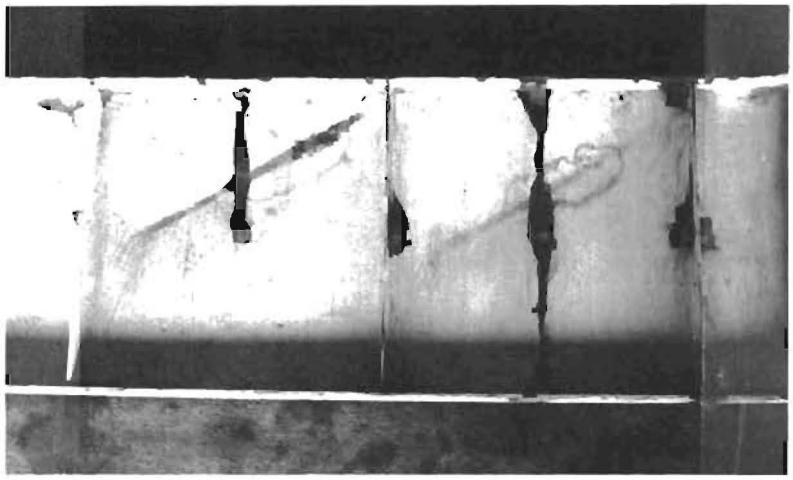

Fig. 3.5 Mode of Failure of $\alpha = 1.0$
Panel Girder HS-1A, T2

Fig. 3.6 Mode of Failure of $\alpha = 0.5$
Panel Girder HS-1A, T3

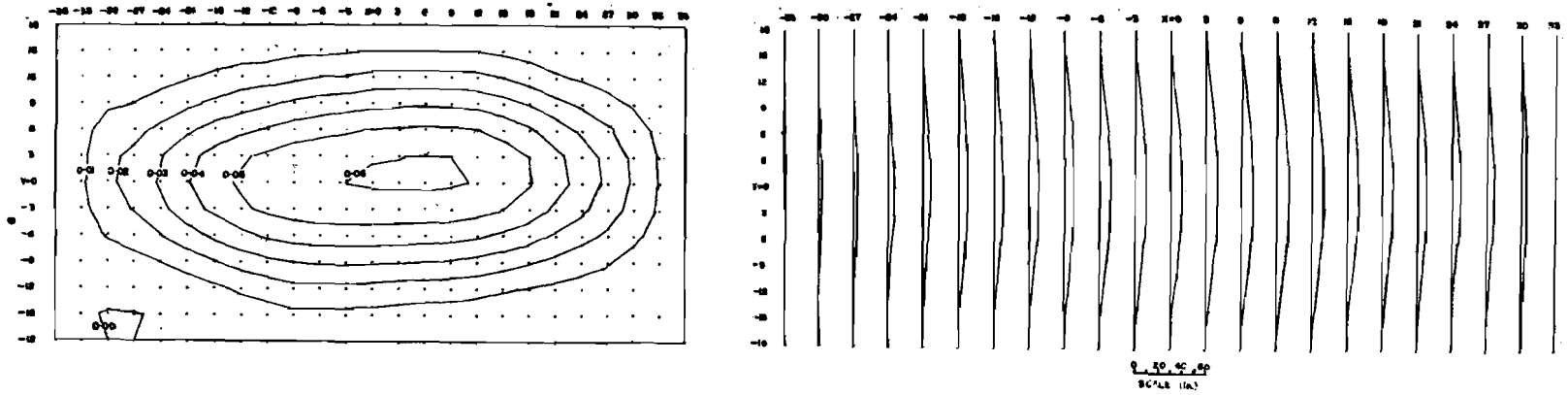

P = 0 kip

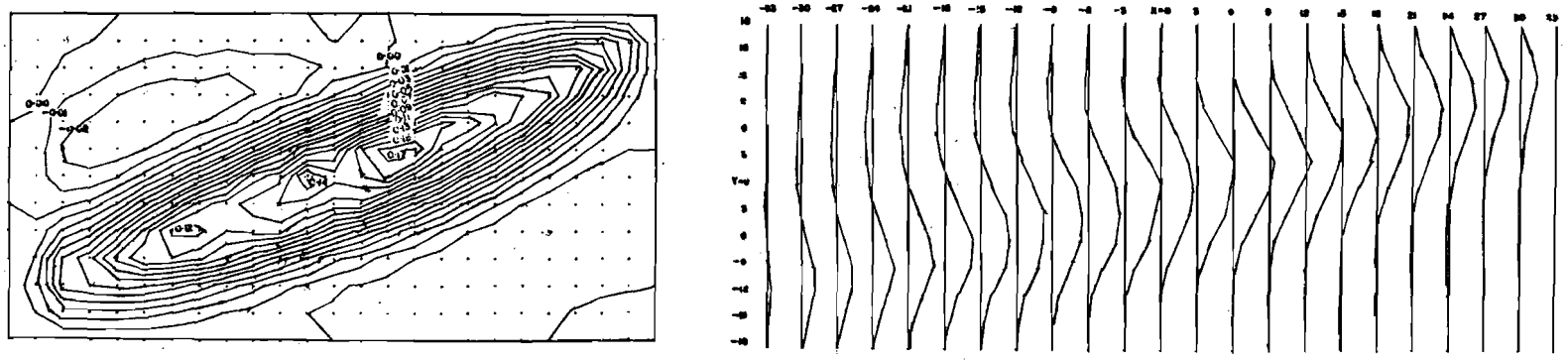

P = 98 kips

Fig. 3.7 Web Deflection Contours and Profile Plots of Girder HS-1A, α = 2.0 Panel

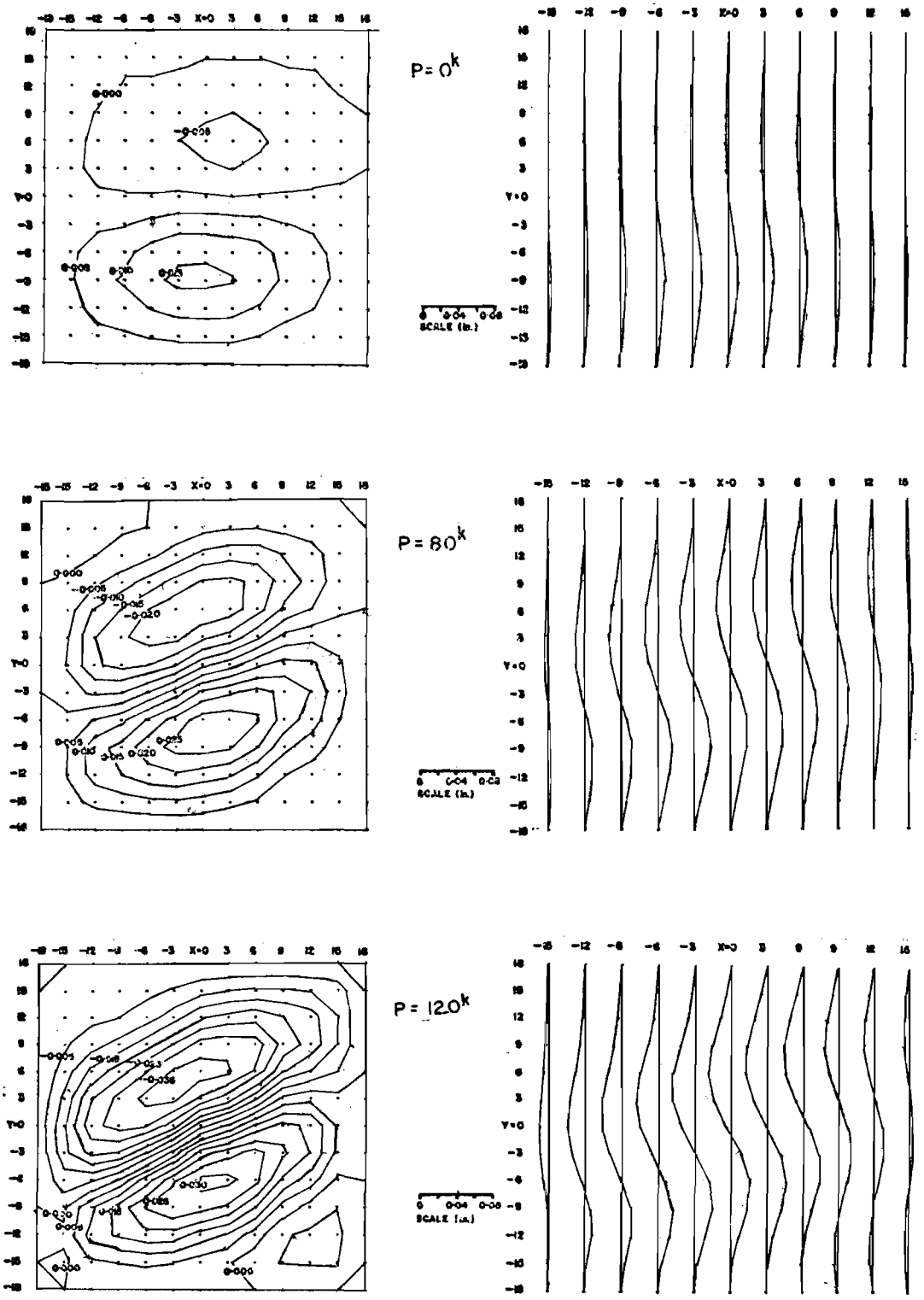

Fig. 3.8 Web Deflection Contours and Profile Plots of Girder HS-1A, α = 1.0 Panel

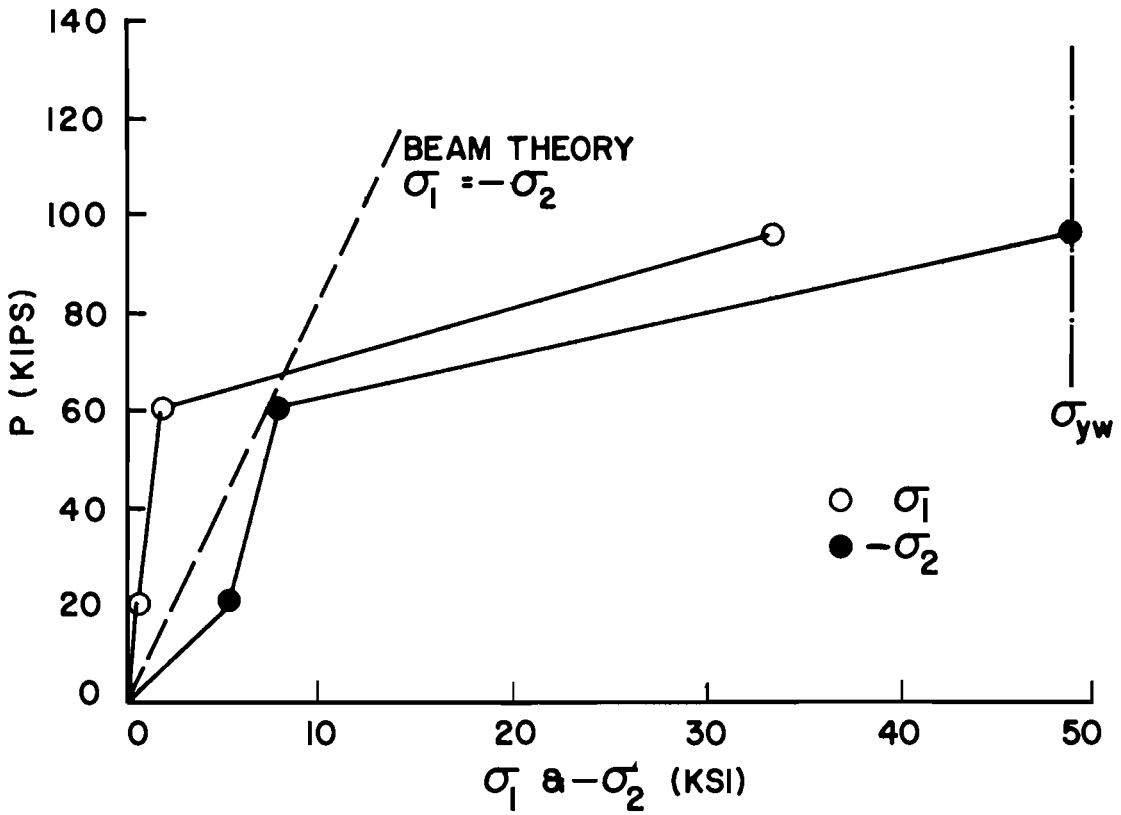

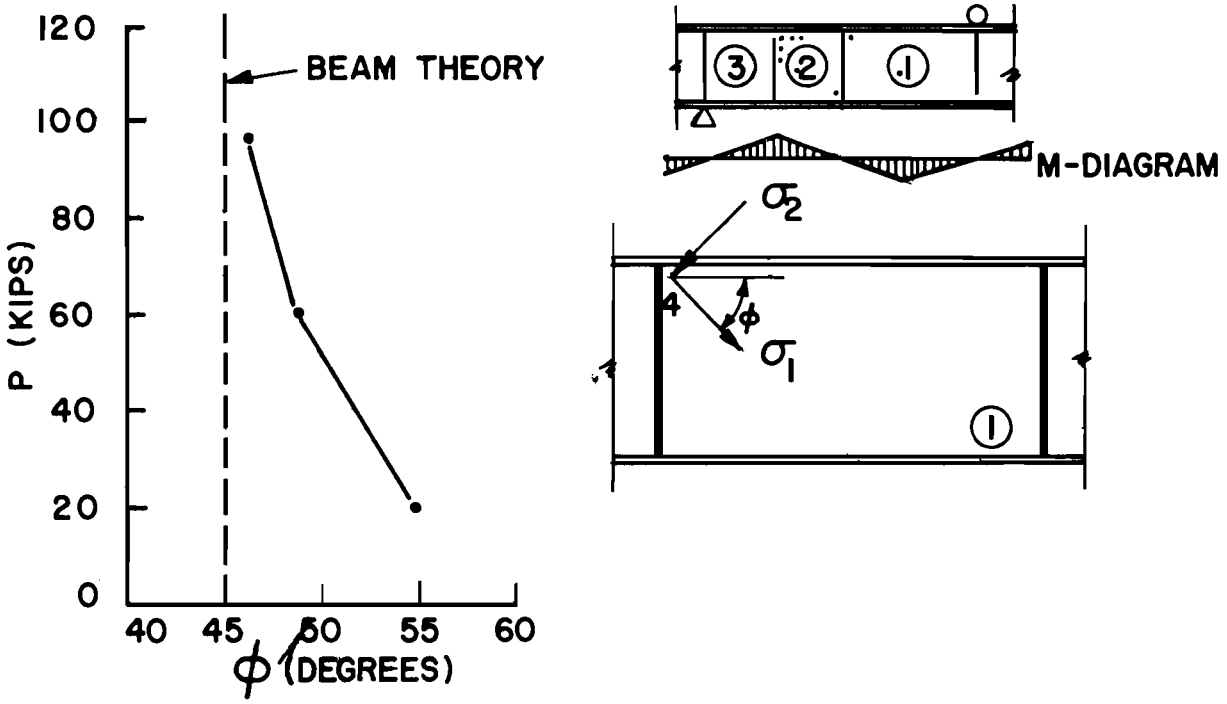

Fig. 3.9 Principal Stresses in $\alpha = 2.0$ Panel, T1

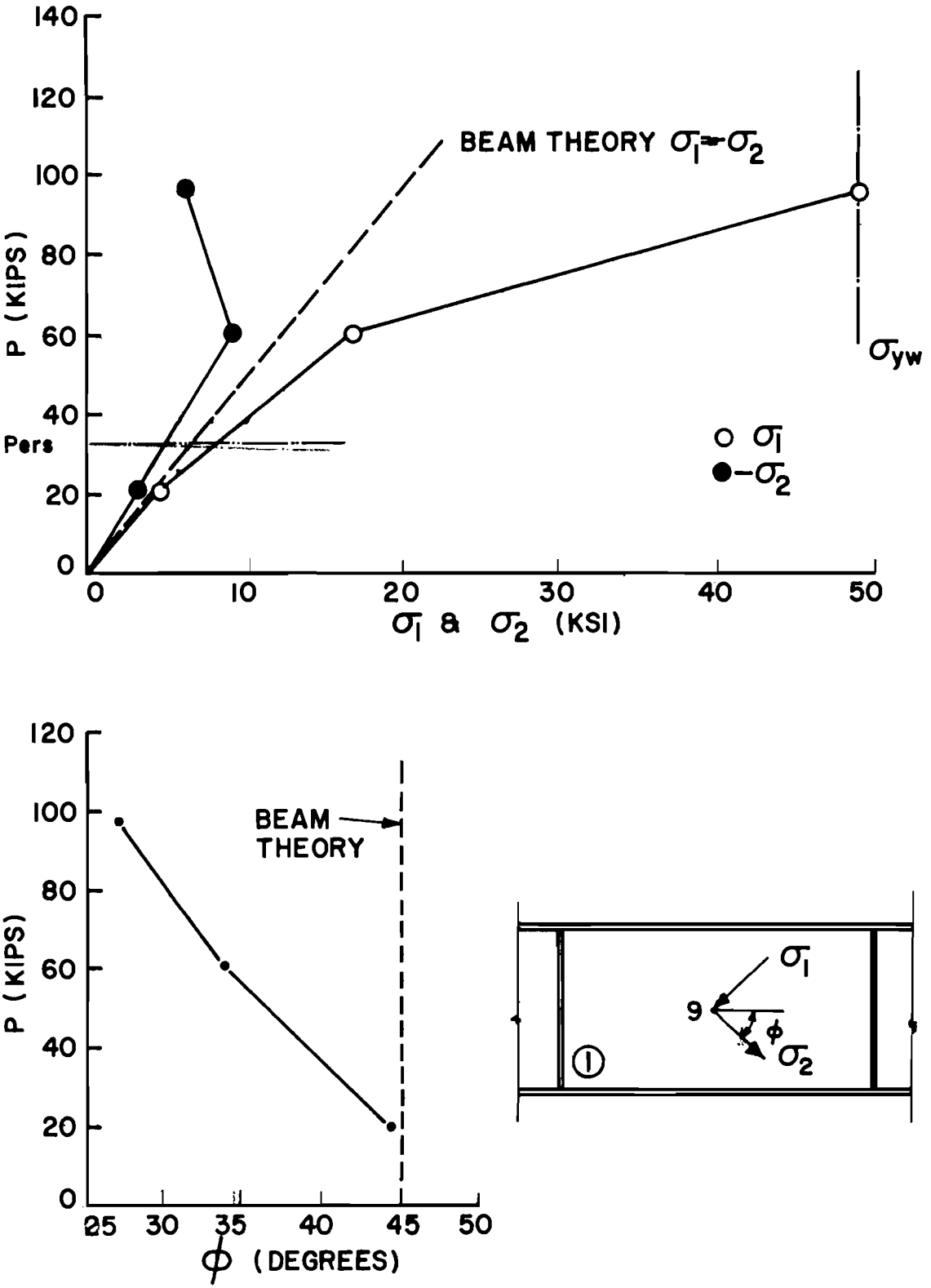

Fig. 3.10 Principal Stresses in $\alpha = 2.0$ Panel, T1

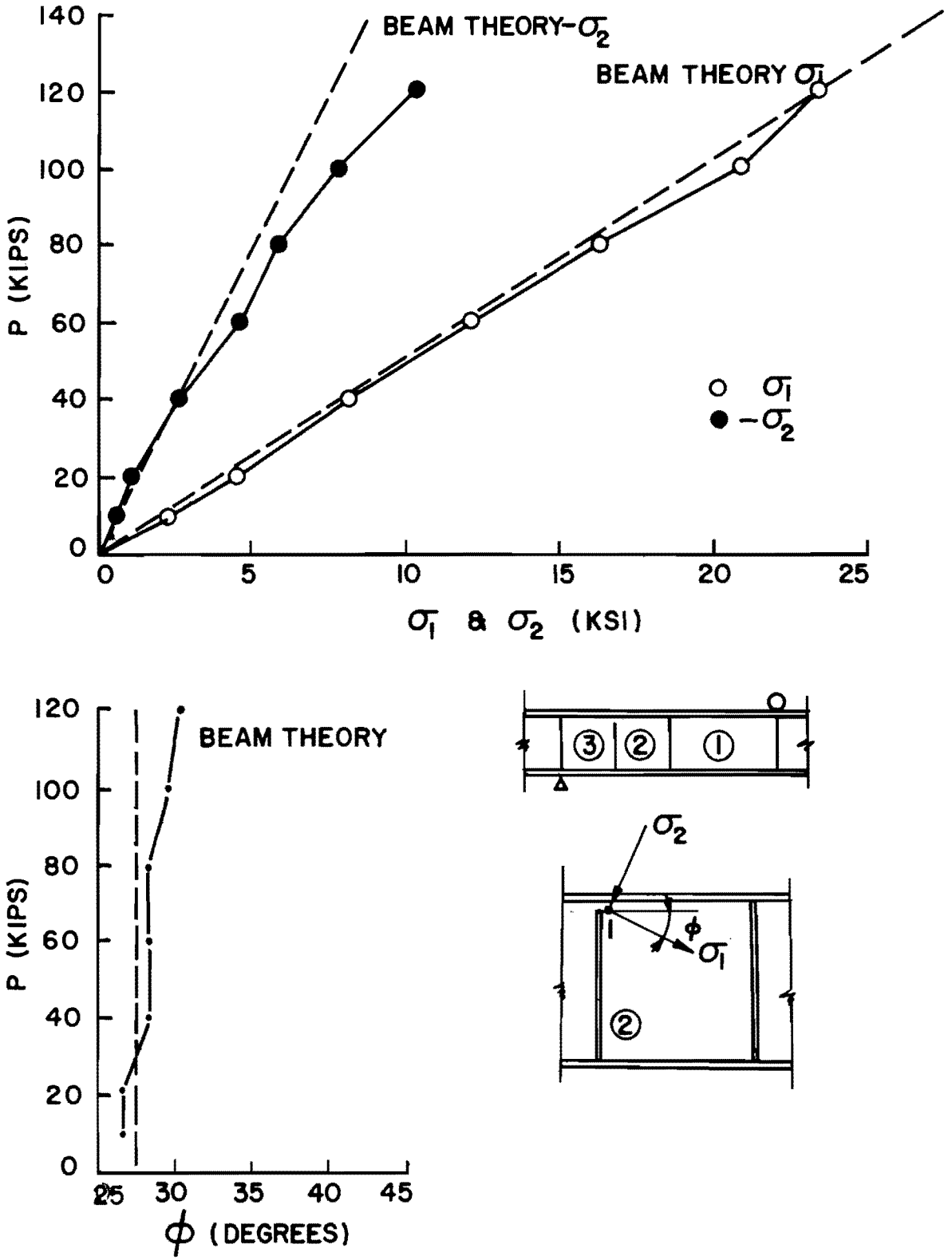

Fig. 3.11 Principal Stresses in $\alpha = 1.0$ Panel, T2

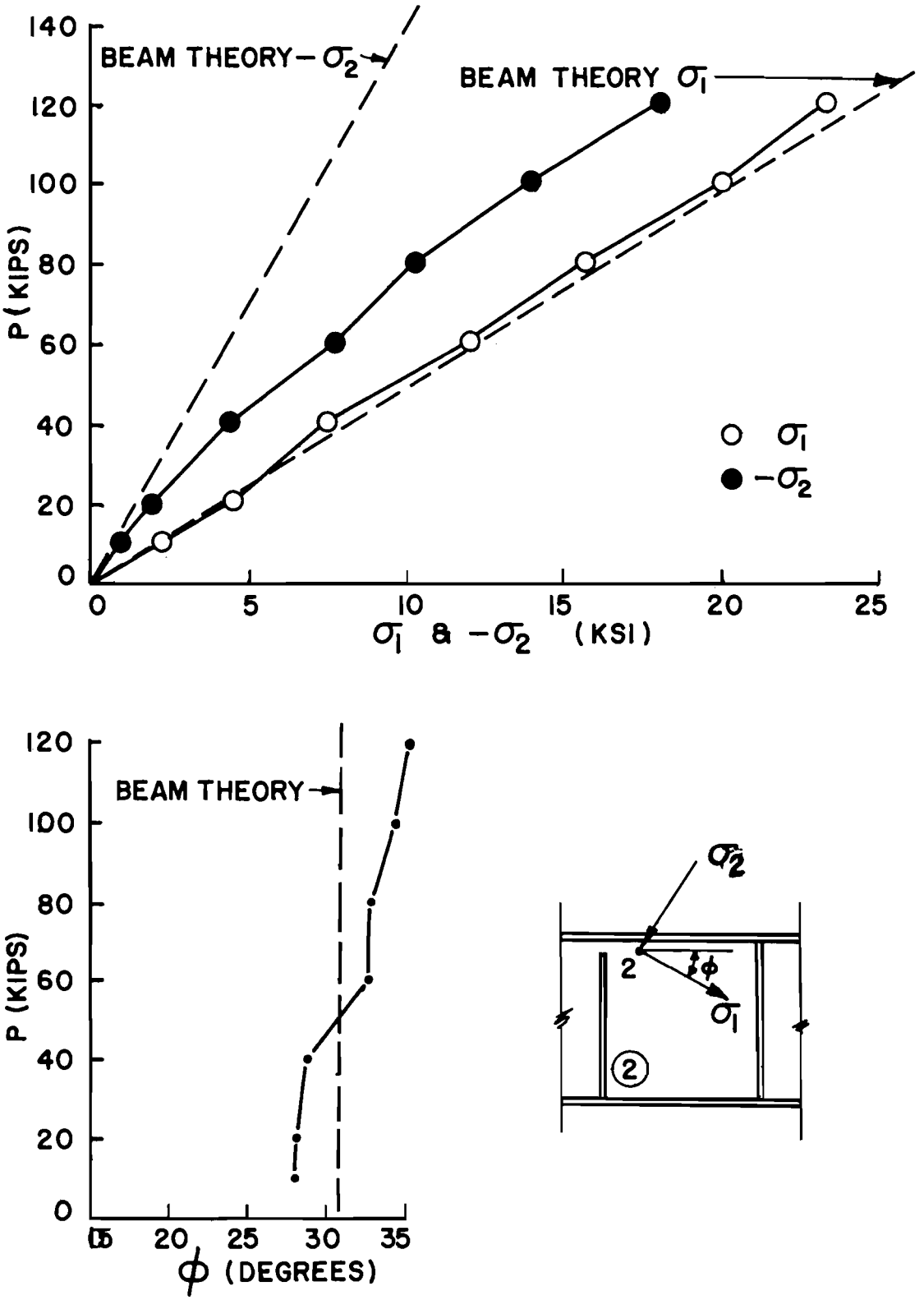

Fig. 3.12 Principal Stresses in α = 1.0 Panel, T2

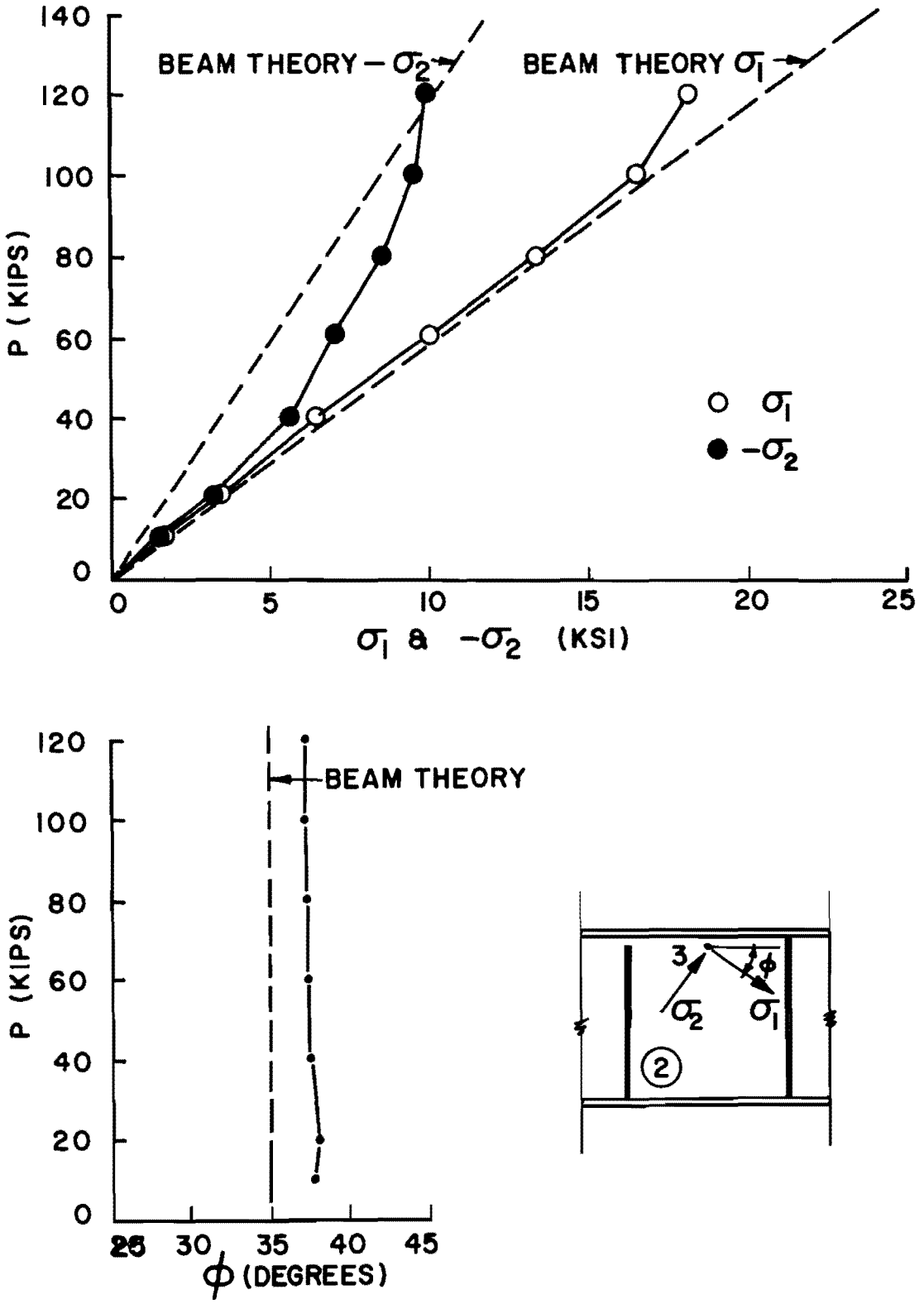

Fig. 3.13 Principal Stresses in α = 1.0 Panel, T2

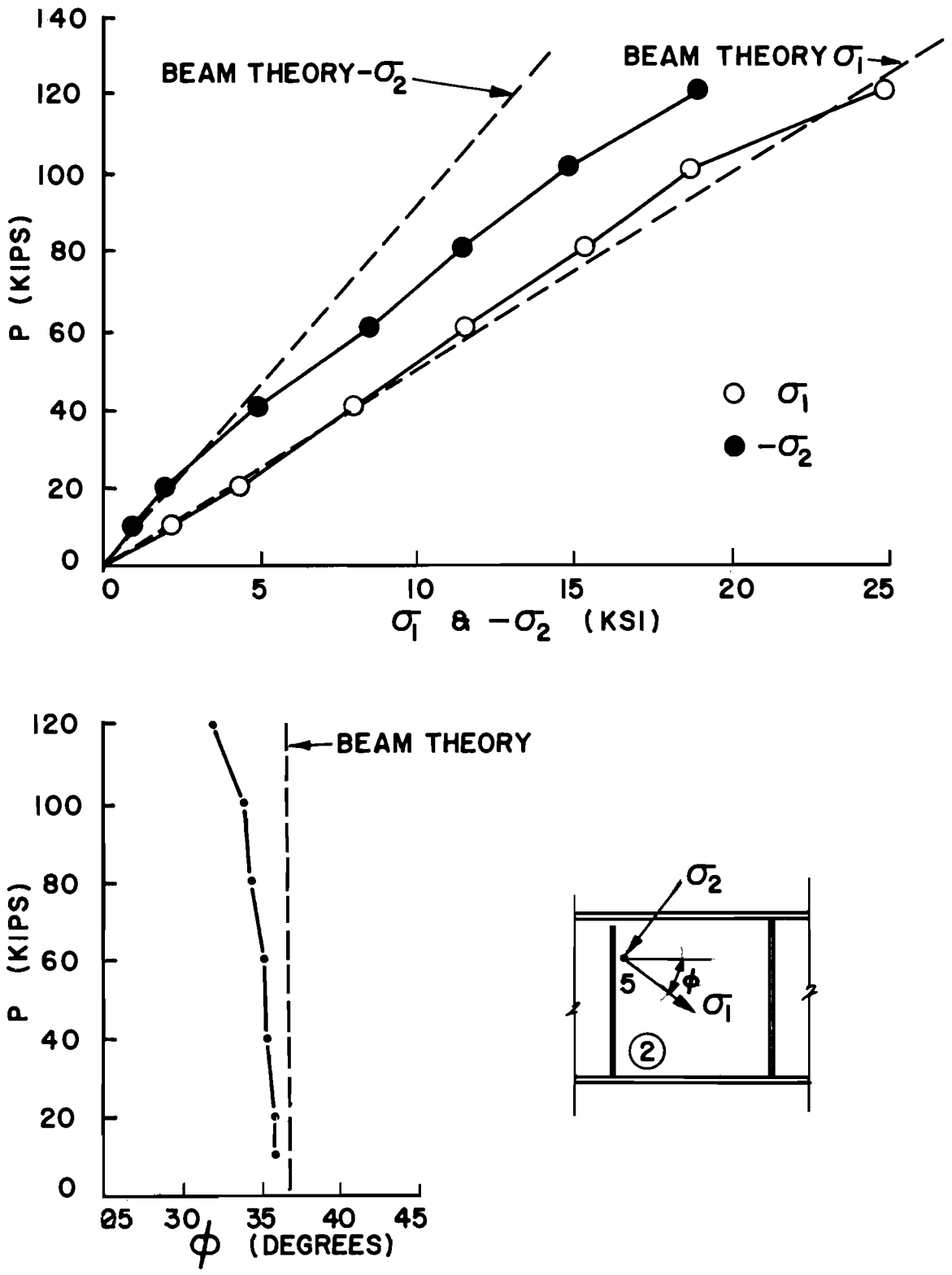

Fig. 3.14 Principal Stresses in $\alpha = 1.0$ Panel, T2

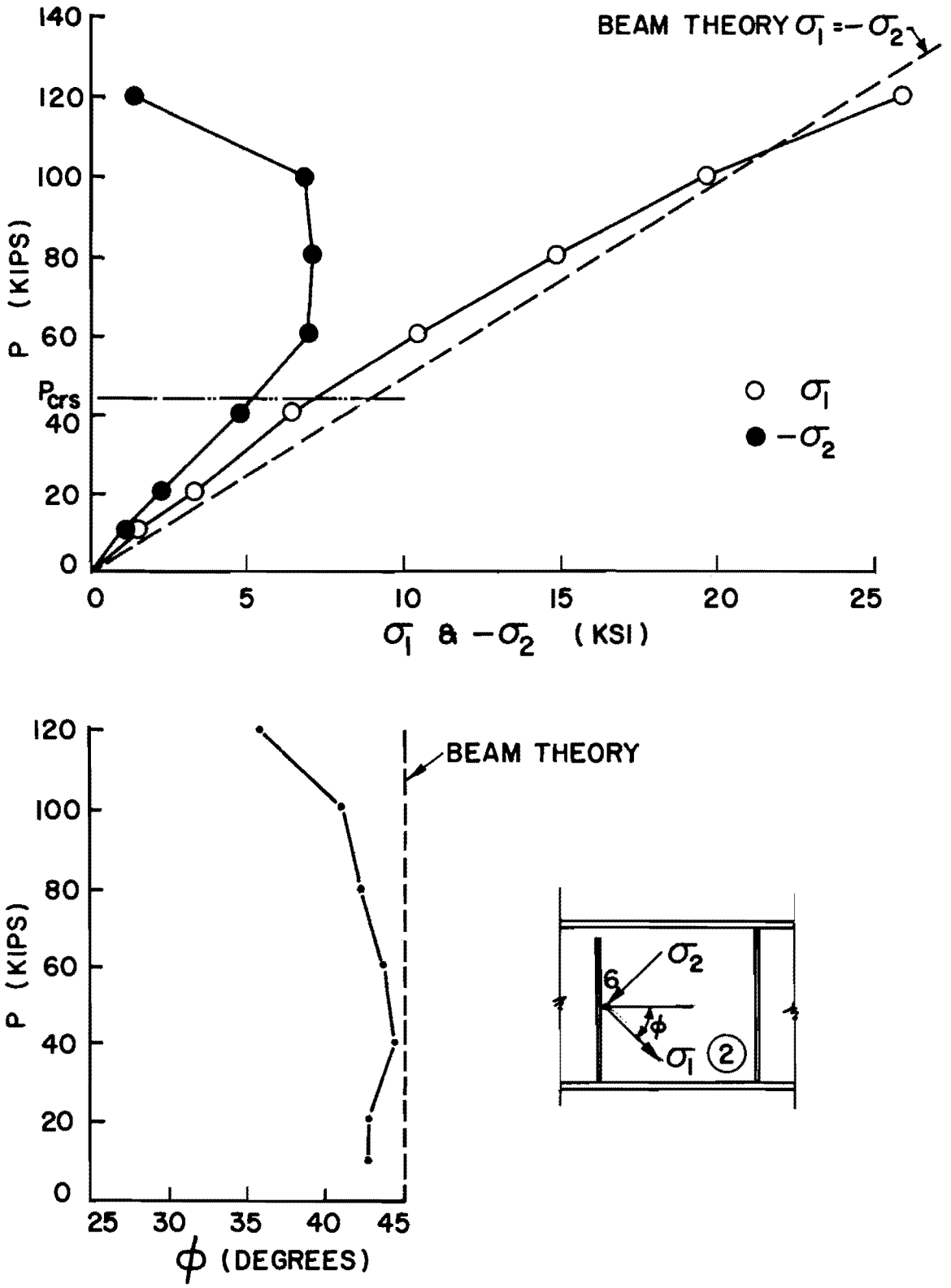

Fig. 3.15 Principal Stresses in $\alpha = 1.0$ Panel, T2

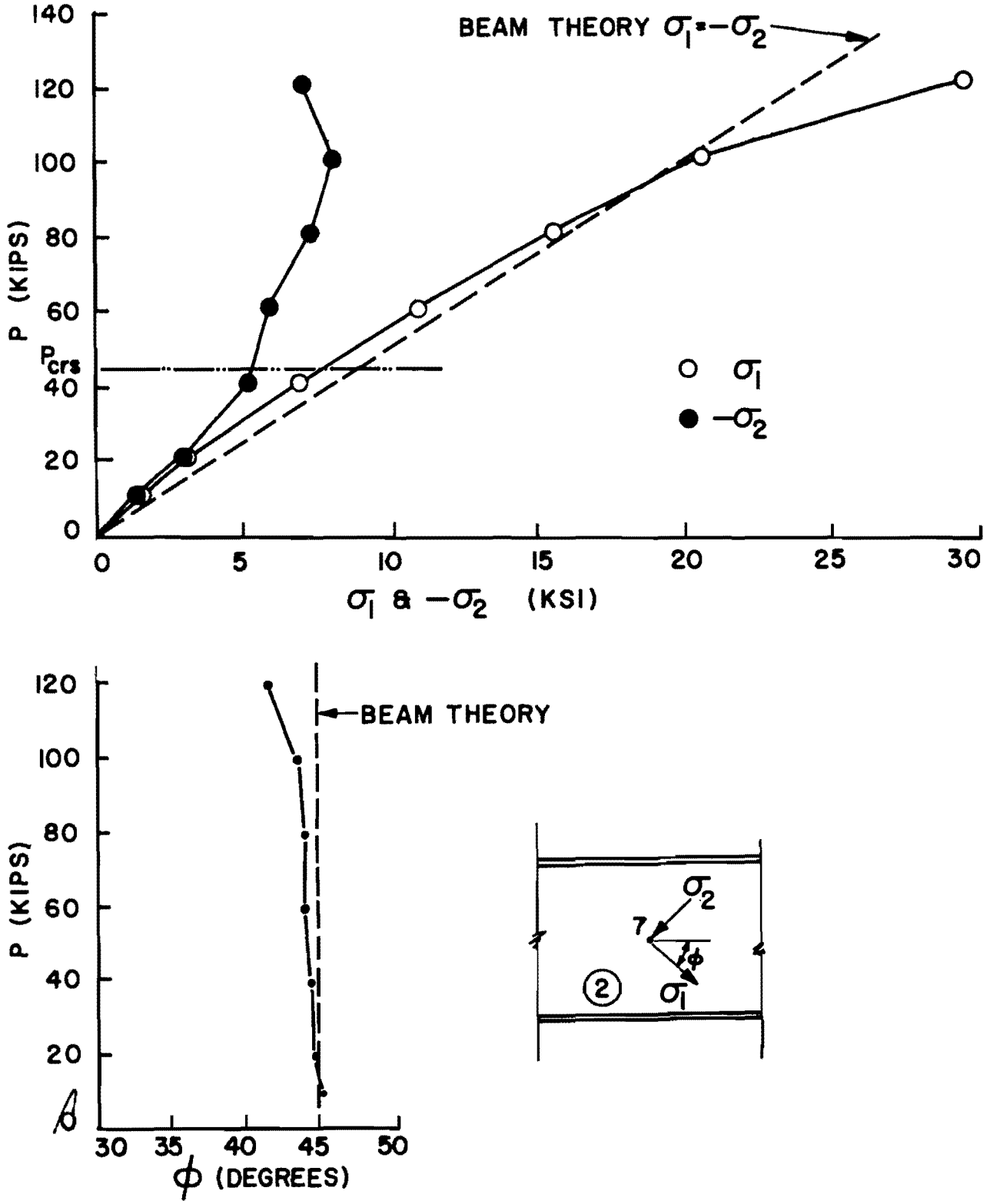

Fig. 3.16 Principal Stresses in $\alpha = 1.0$ Panel, T2

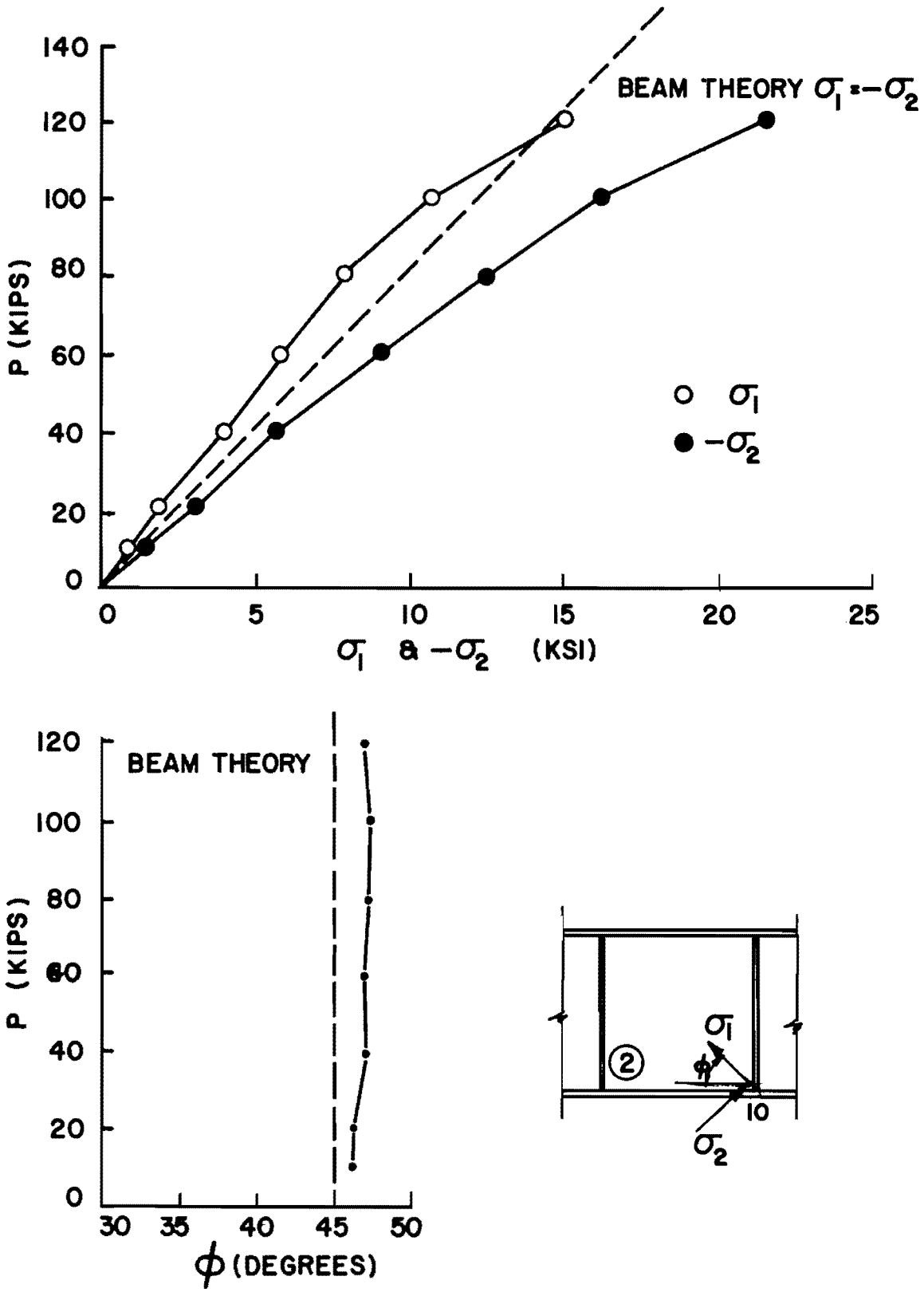

Fig. 3.17 Principal Stresses in $\alpha = 1.0$ Panel, T2